Comput Geosci (2013) 17:325–350
DOI 10.1007/s10596-012-9333-z

ORIGINAL PAPER

Investigation of the sampling performance of ensemble-based methods with a simple reservoir model

Alexandre A. Emerick · Albert C. Reynolds

Received: 17 January 2012 / Accepted: 21 November 2012 / Published online: 5 January 2013

Abstract The application of the ensemble Kalman filter (EnKF) for history matching petroleum reservoir models has been the subject of intense investigation during the past 10 years. Unfortunately, EnKF often fails to provide reasonable data matches for highly nonlinear problems. This fact motivated the development of several iterative ensemble-based methods in the last few years. However, there exists no study comparing the performance of these methods in the literature, especially in terms of their ability to quantify uncertainty correctly. In this paper, we compare the performance of nine ensemble-based methods in terms of the quality of the data matches, quantification of uncertainty, and computational cost. For this purpose, we use a small but highly nonlinear reservoir model so that we can generate the reference posterior distribution of reservoir properties using a very long chain generated by a Markov chain Monte Carlo sampling algorithm. We also consider one adjoint-based implementation of the randomized maximum likelihood method in the comparisons.

Keywords Uncertainty quantification · History matching · Ensemble Kalman filter · Ensemble smoother · Randomized maximum likelihood · Markov chain Monte Carlo

A. A. Emerick (✉)
Petrobras. Av. Horacio de Macedo 950, Cid. Universitaria, Rio de Janeiro, RJ 21941-915, Brazil
e-mail: aemerick@gmail.com

A. C. Reynolds
Univ. of Tulsa, 800 South Tucker Drive, Tulsa, OK 74104, USA
e-mail: reynolds@utulsa.edu

1 Introduction

Reservoir simulation is a valuable tool for the decision-making process involved in the development and management of petroleum reservoir exploitation projects. However, because simulation models are constructed with poorly known reservoir properties, it is essential to properly characterize the uncertainty in their predictions to manage risk. Bayesian statistics provides an adequate framework for quantifying uncertainty. The starting point is the Bayes' theorem, which allows us to construct the conditional probability density function (PDF) of a set of poorly known model parameters conditional to noisy measurements. Then, the problem of quantifying uncertainty can be replaced by the conceptually simpler problem of sampling this PDF. However, rigorously sampling this PDF can be complex and computationally expensive; thus, only approximate sampling methods are practical. Markov chain Monte Carlo (MCMC) is known to be a rigorous sampling procedure; however, its direct application to realistic reservoir problems is not feasible with the computational power currently available [3, 31, 37]. Randomized maximum likelihood (RML) [23, 38, 41] is an approximate sampling method which has been successfully applied to reservoir history-matching problems [16, 31, 51, 59]. RML requires solving one minimization problem for each sample, which seems to be computationally feasible only with a gradient-based optimization method. However, efficient calculation of gradients requires the implementation of the adjoint method [5, 6, 28, 58], which, unfortunately, is not commonly available in commercial reservoir simulators. Recently, the ensemble Kalman filter (EnKF) [4, 12, 20] and related methods have emerged as very

attractive alternatives for reservoir history-matching problems. The main advantages of these methods include their computational efficiency and the ease of implementation. In fact, because ensemble-based methods typically do not require adjoint code, they can be coupled with virtually any commercial reservoir simulator. Moreover, they can be easily adapted to different types of data and model variables.

In this paper, we compare the sampling performance of one adjoint-based and nine ensemble-based methods for a small, but highly nonlinear, reservoir history-matching problem. This paper was inspired by the early work of Liu and Oliver [31], in which the results of a very long Markov chain were used as the reference results to compare the performances of the following methods: linearization about the MAP, RML, and the pilot point method [8, 25, 26]. Liu [30] included the gradual deformation method [22, 45] in this comparative study. The authors concluded that RML was the only approximate sampling method which gave an acceptable quantification of uncertainty.

This paper is organized as follows: in the next section, we formulate the uncertainty quantification problem in terms of sampling a posterior PDF. Next, we introduce our test problem, which consists of a one-dimensional reservoir with two-phase flow. Then, we present a separate section for each sampling method. Each section contains a short description of the method, followed by the corresponding sampling results. We first present MCMC, which serves as reference for the comparisons, followed by RML, EnKF, deterministic EnKF (DEnKF) [47], half-iteration EnKF (HI-EnKF) [56], Lorentzen–Nævdal iterative EnKF (LN-IEnKF) [32], Krymskaya–Hanea–Verlaan iterative EnKF (KHV-IEnKF) [24], EnKF-MCMC [9], ensemble smoother (ES) [55], ES with multiple data assimilation (ES-MDA) [10] and the ensemble randomized maximum likelihood (EnRML) [18]. After that, we present a section with a discussion of the overall performance of these methods. The last section of the paper presents the conclusions.

2 Posterior PDF and objective function

For the purpose of quantifying uncertainty, it suffices to sample the posterior PDF of reservoir model parameters conditional to the observations. For a Gaussian prior and Gaussian measurement errors, it can be shown that the posterior PDF, $f(m|d_{\text{obs}})$, has the following form [39, Chap. 8]:

$$\pi(m) \equiv f(m|d_{\text{obs}}) = a \exp\left(-O(m)\right), \tag{1}$$

where a is a normalizing constant and $O(m)$ is the objective function given by

$$O(m) = \frac{1}{2}\left(m - m_{\text{pr}}\right)^{\text{T}} C_{\text{M}}^{-1}\left(m - m_{\text{pr}}\right) + \frac{1}{2}\left(d - d_{\text{obs}}\right)^{\text{T}} C_{\text{D}}^{-1}\left(d - d_{\text{obs}}\right). \tag{2}$$

In the above equations, m is the N_m-dimensional vector of model parameters, m_{pr} is the prior mean, C_{M} is the $N_m \times N_m$ prior covariance matrix, d is the N_d-dimensional vector of predicted data, and d_{obs} is the corresponding vector of observed data. C_{D} is the $N_d \times N_d$ covariance matrix of the measurement errors.

According to Oliver et al. [39, Chap. 8], the objective function normalized by the number of data points evaluated at samples of the posterior PDF should approximately satisfy the following condition:

$$O_{\text{N}} \equiv \frac{O(m)}{N_d} \leq 1 + 5\sqrt{\frac{2}{N_d}}. \tag{3}$$

3 Test problem

The test problem is a one-dimensional reservoir model under waterflooding (Fig. 1). The number of gridblocks is 31 and the dimensions of all gridblocks are 50 ft $\times$ 50 ft $\times$ 50 ft. The model parameters are gridblock log-permeabilities, $\ln(k)$. The "true" permeability field (Fig. 2a) was generated using an exponential covariance function with a practical range corresponding to the size of ten gridblocks. The prior mean of $\ln(k)$ is 5.0 and the prior variance is equal to 1.0 for all gridblocks. The porosity is constant and equal to 0.25; the oil viscosity is 2 cP and the water viscosity 1 cP. The initial reservoir pressure is 3,500 psi and the compressibility of oil, water, and rock is 10^{-5}, 10^{-6}, and 5×10^{-6} psi^{-1}, respectively. In this synthetic reservoir, there is a water injection well in the first gridblock which is operated at a constant bottomhole pressure of 4,000 psi. In the last gridblock, there is a producing well operated at a constant bottomhole pressure of 3,000 psi. The observations correspond to gridblock pressures at a monitor well located in the center of the

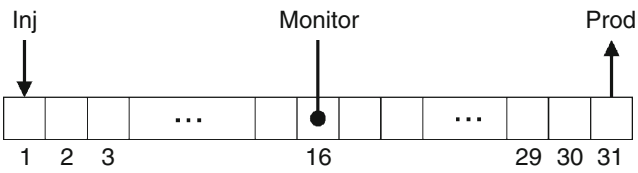

Fig. 1 Gridblocks and well locations

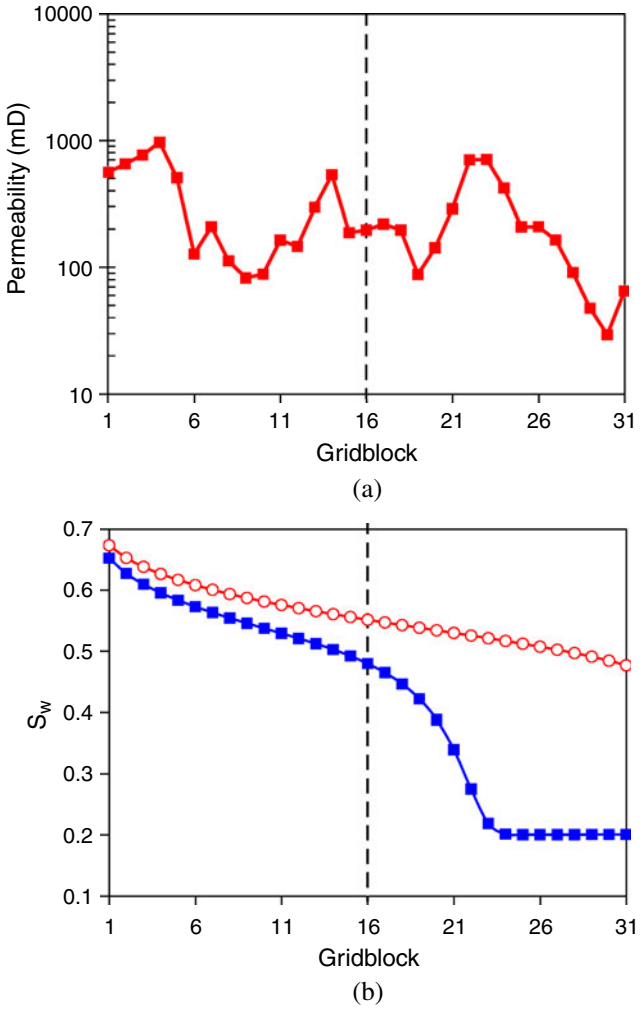

Fig. 2 **a** Permeability of the true model. **b** Water saturation at the end of the historical period (in *blue*) and at the end of the forecast period (in *red*). The *vertical dashed line* indicates the position of the monitor well

reservoir (gridblock number 16). The historical period corresponds to 360 days, with one pressure measurement every 30 days, which results in 12 data points. We added random Gaussian noise with mean equal to zero and standard deviation equal to 1 psi to the data predicted by the true model to define the "measurements." The historical period was defined such that we have water breakthrough at the monitor well but not at the producing well. Figure 2b shows the water saturation distribution at the end of the history (360 days) and at the end of a forecast period (750 days). Our objective was to create a reservoir history-matching problem that was challenging for data assimilation yet was also small enough so one could afford to generate the correct posterior distribution of the vector of model parameters and performance predictions using MCMC. Thus, we made the test problem highly nonlinear by assimilating only pressure data with a small noise level and predicting the water production rate.

Using the same covariance function and the same prior mean to construct the true model, we generated ten different prior ensembles of $\ln(k)$ with 100 models each. These ensembles were used in all ensemble-based methods presented in the following sections. It is not the objective of this paper, however, to investigate the effect of the ensemble size in the performance of the methods. Note that with an ensemble consisting of 100 realizations, the number of ensemble members is more than three times larger than the number of model parameters. Therefore, an ensemble size of 100 should be sufficiently large for data assimilation without resorting to standard ad hoc fixes such as covariance inflation [2, 14] and covariance localization [20, 21, 46], which are designed to control the negative consequences of sampling error and low rank covariance matrices when the number of model parameters is far greater than the number of ensemble members. The study of such ad hoc fixes is not the focus in this paper.

4 Markov chain Monte Carlo

Here, we apply the Metropolis–Hastings MCMC algorithm [19, 34] to sample the posterior PDF, $\pi(m)$, given by Eq. 1. The steps of this MCMC algorithm follow:

1. Set $k = 0$, where k is the proposal index of the Markov chain. Select the initial model of the chain, $m_k = m_0$.
2. Propose a new model, $\widehat{m}_{k+1}$, by sampling the PDF $q(m_k, \widehat{m}_{k+1})$, which represents the "probability" of proposing a transition from the model m_k to $\widehat{m}_{k+1}$.
3. Compute the probability of accepting the proposal as

$$\alpha\left(m_k, \widehat{m}_{k+1}\right) = \min\left\{1, \frac{q\left(\widehat{m}_{k+1}, m_k\right)\pi\left(\widehat{m}_{k+1}\right)}{q\left(m_k, \widehat{m}_{k+1}\right)\pi\left(m_k\right)}\right\}. \tag{4}$$

4. Sample u from a uniform distribution on $[0, 1]$. If $u \leq \alpha(m_k, \widehat{m}_{k+1})$, accept the proposal, i.e., set $m_{k+1} = \widehat{m}_{k+1}$. Otherwise, repeat the old model in the chain, i.e., set $m_{k+1} = m_k$.
5. Set $k = k + 1$ and return to step 2.

In this paper, we use a proposal mechanism based on local perturbations around the current model of the chain [17]. In this procedure, we write the transition probability, $q(m_k, \widehat{m}_{k+1})$, as a Gaussian centered at the current model, m_k, with the scaled covariance,

$\sigma^2 C_M$, where $\sigma < 1$ is a scaling factor. In this case, each proposal can be written as

$$\widehat{m}_{k+1} = m_k + C_M^{1/2} \delta z, \tag{5}$$

where δz is a sample from the Gaussian $\mathcal{N}(0, \sigma^2 I_{N_m})$, with I_{N_m} denoting the N_m-dimensional identity matrix. This procedure leads to a symmetric transition probability, i.e., $q(m_k, \widehat{m}_{k+1}) = q(\widehat{m}_{k+1}, m_k)$. Therefore, the probability of accepting the proposal (Eq. 4) simplifies to

$$\alpha\left(m_k, \widehat{m}_{k+1}\right) = \min\left\{1, \frac{\pi\left(\widehat{m}_{k+1}\right)}{\pi\left(m_k\right)}\right\}. \tag{6}$$

The scaling factor, σ, controls the performance of the chain. Small values of σ lead to high acceptance rates but poor mixing. High values of σ, on the other hand, lead to low acceptance rates. Although the optimal choice of σ depends on the target PDF, several papers (e.g., Gelman et al. [17], Roberts et al. [43], Roberts and Rosenthal [44]) have provided theoretical and empirical results showing that in high dimensions, it is optimal to choose σ such that the acceptance rate of the chain is approximately 0.234.

For the test problem, we generate a long Markov chain with 20 million proposals. Note that each proposal requires one reservoir simulation, but because we have an extremely small problem, where each reservoir simulation takes approximately 0.2 s, it is feasible to generate a very long chain. Here, we assume that this chain is long enough to provide a reasonable sampling of the posterior PDF, which serves as the reference for our comparisons. Figure 3 presents the values O_N for the accepted models in the chain after a transitional period (burn-in). The total number of accepted models is 458,648. This gives an acceptance rate of 0.229, which is close to the "optimal" acceptance rate of 0.234. In MCMC, we used a scaling factor $\sigma = 0.05$. This scaling factor was chosen after some experimentation.

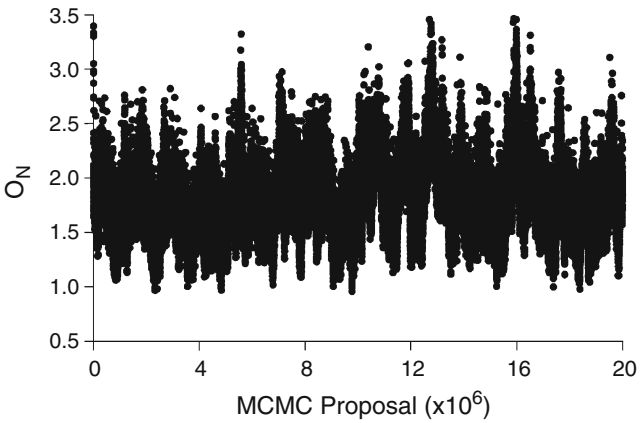

Fig. 3 Normalized objective function of every 100th accepted model in the Markov chain

Figure 4a presents the distribution of permeability (percentiles P2, P25, P50, P75, and P98) obtained from MCMC. The results in this figure show a narrow distribution of permeability for the gridblocks to the left of the monitor well. The spread increases for the gridblocks to the right of the monitor well. Figure 4b shows the distributions (percentiles P2, P25, P50, P75, and P98) of predicted water rate at the producing well (q_w). This figure indicates that there is a relatively small uncertainty in q_w. Also, q_w obtained with the true model is above the percentile P75 obtained with MCMC.

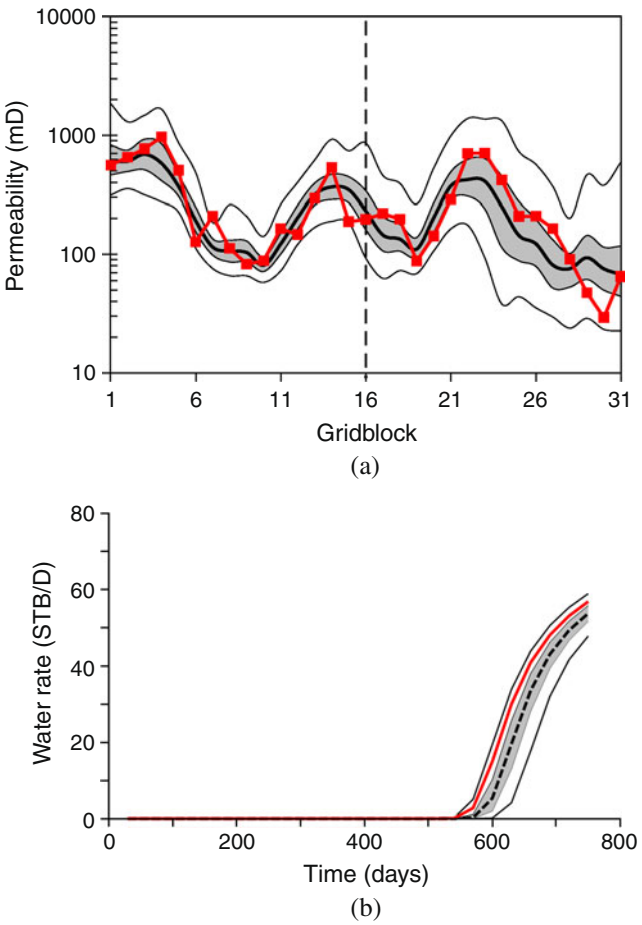

Fig. 4 Distributions of permeability (**a**) and water production rate (**b**) obtained from MCMC. In **a**, the *red curve with solid squares* is the true permeability field, the *solid black curve* is the median, the *gray-shaded area* corresponds to the region between the percentiles P25 and P75, and the *external bounding curves* are the percentiles P2 and P98. In **b**, the *red curve* is the prediction obtained with the true model, the *dashed curve* is the median, and the *gray-shaded area* corresponds to the region between the percentiles P25 and P75. The *external bounding curves* are the percentiles P2 and P98

5 Randomized maximum likelihood

RML was independently introduced by Kitanidis [23] and Oliver et al. [38] as an approximate sampling method. To obtain the jth sample, $m_{c,j}$, of the posterior PDF using RML, we solve the minimization problem

$$m_{c,j} = \arg\min_m O_j(m), \tag{7}$$

where

$$O_j(m) = \frac{1}{2}\left(m - m_{uc,j}\right)^T C_M^{-1}\left(m - m_{uc,j}\right) + \frac{1}{2}\left(d - d_{uc,j}\right)^T C_D^{-1}\left(d - d_{uc,j}\right). \tag{8}$$

In Eq. 8, $m_{uc,j}$ is a sample from $\mathcal{N}(m_{pr}, C_M)$ and $d_{uc,j}$ is a sample from $\mathcal{N}(d_{obs}, C_D)$; the remaining terms were defined before.

In our implementation, we solve this minimization problem using the LBFGS algorithm [15, 36, 60] with scaling [29, 60] and bracketing cubic line search [39, Chap. 8]. We control possible overcorrection in the model by restricting the step size at early iterations. Specifically, we limit the maximum step size normalized by the 2-norm of the search direction to 0.25 until we obtain $O_N < 1{,}000$. We also apply damping to the objective function [15, 28] by artificially multiplying the standard deviation of the measurement errors by three until the minimization reduces O_N to 5.0. After that, we remove the damping and continue the minimization with the actual standard deviations of the measurement errors. The gradients are computed using the adjoint method [5, 6, 28, 58]. For convergence, we require both the change in the objective function and the change in the vector of model parameters over an iteration to be small, i.e.,

$$\frac{|O(m^{\ell+1}) - O(m^{\ell})|}{O(m^{\ell})} < 10^{-4} \tag{9}$$

and

$$\max_{1\le i\le N_m}\left|\frac{m_i^{\ell+1} - m_i^{\ell}}{m_i^{\ell}}\right| < 10^{-3}, \tag{10}$$

where the superscript ℓ denotes the iteration index.

Using RML, we sampled the posterior PDF by generating ten ensembles of 100 conditional realizations each. Figure 5a presents the permeabilities of the first ensemble, and Fig. 5b shows the distributions of permeability obtained by combining the ten ensembles. The results in Fig. 5 indicate that RML obtains a distribution of permeability reasonably close to the distribution

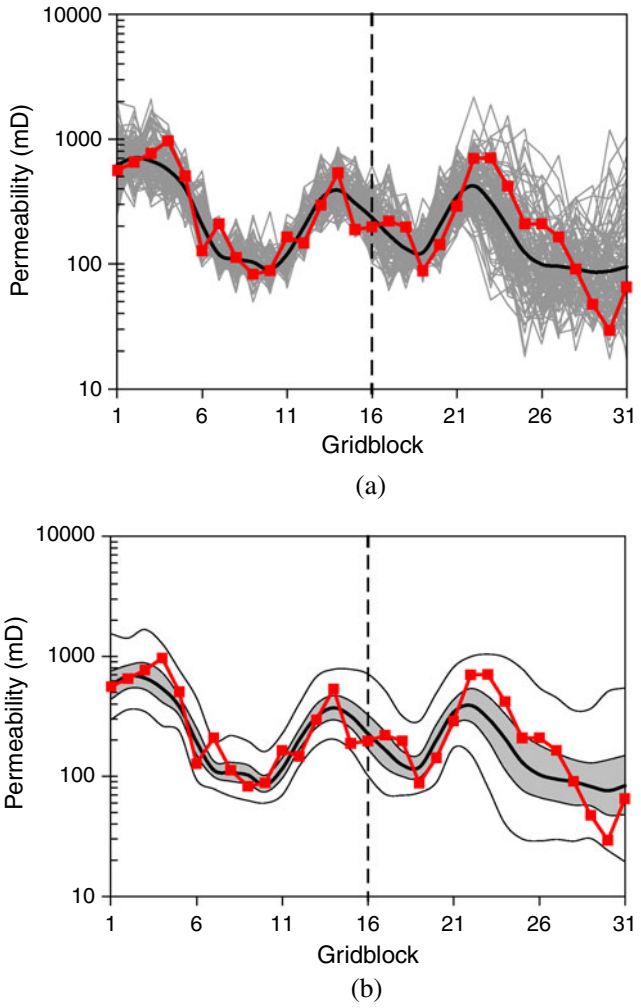

Fig. 5 Permeability after RML. **a** First ensemble. The *solid black curve* is the ensemble mean and the *gray curves* are the ensemble members. **b** All ensembles. The *solid black curve* is the median, the *gray-shaded area* corresponds to the region between the percentiles P25 and P75, and the *external bounding curves* are the percentiles P2 and P98. The true permeability field is included in both plots (*red curve with solid squares*)

obtained from MCMC. Figure 6a presents the box plots of cumulative water production (W_p) after 750 days obtained from each of the ten RML ensembles. In this figure, we also present the box plot obtained from MCMC. Figure 6a shows that RML results in distributions of W_p very close to the distribution obtained with MCMC. It is important to note that Fig. 6a also indicates that distributions obtained by the ten different RML runs are mutually consistent, i.e., there are no significant differences between these ten distributions. Although we did not present the results for all ten ensembles individually, the same conclusion about consistency applies to the resulting permeability fields. This consistency indicates that one ensemble of 100 models

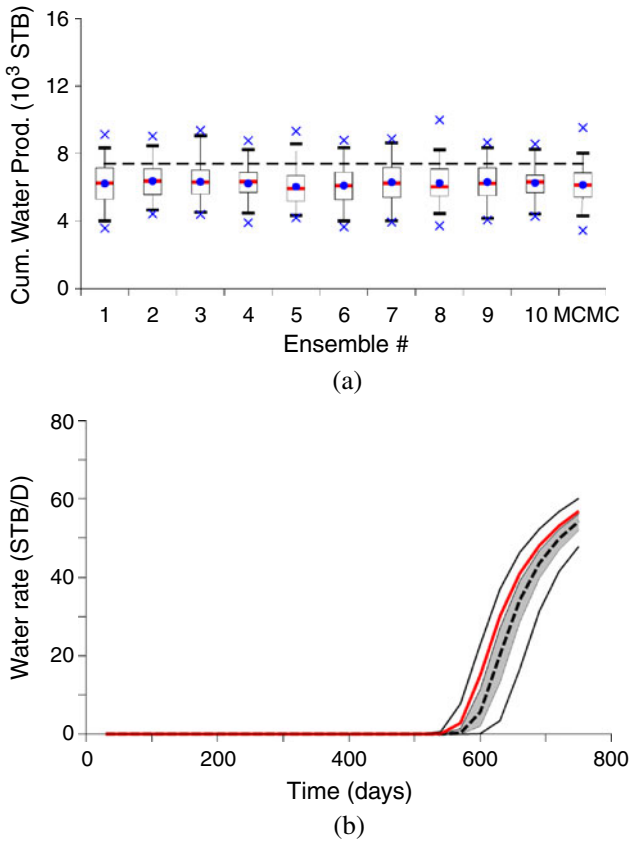

Fig. 6 Water production after RML. **a** Box plot of cumulative water production, W_p, for each ensemble. The *horizontal dashed line* indicates the water production obtained with the true model. The *red line* within each box corresponds to the median, and the *bottom and top* of each box correspond to the percentiles P25 and P75. The *ending points* of the box plots correspond to the percentiles P2 and P75. The *blue dots* correspond to the mean and the *crosses* correspond to the minimum and maximum values. **b** Water production rate, q_w, distributions obtained by combining the ten ensembles. The *solid red curve* is the prediction obtained with the true model, the *dashed curve* is the median, and the *gray-shaded area* corresponds to the region between the percentiles P25 and P75. The *external bounding curves* are the percentiles P2 and P98

suffices for the purpose of quantifying uncertainty with RML for this test problem. Figure 6b presents the distribution of q_w obtained by combining the ten RML ensembles. This figure shows that RML also results in a distribution of q_w that is in good agreement with the distribution obtained from MCMC.

6 Ensemble Kalman filter

EnKF was introduced by Evensen [12] and later clarified in [4] and [20]. A convenient way to present EnKF analysis equation is by defining the N_y-dimensional state vector at the nth data assimilation time step, y^n, as

$$y^n = \begin{bmatrix} m^n \\ p^n \end{bmatrix}, \tag{11}$$

where m^n is the N_m-dimensional vector of model parameters and p^n is the N_p-dimensional vector representing the state of the dynamical system (primary variables of the reservoir simulator). The EnKF analysis equation can be written as

$$y_j^{n,a} = y_j^{n,f} + \widetilde{C}_{YD}^{n,f}\left(\widetilde{C}_{DD}^{n,f} + C_D^n\right)^{-1}\left(d_{uc,j}^n - d_j^{n,f}\right), \tag{12}$$

for $j = 1, 2, \cdots, N_e$, with N_e denoting the number of realizations in the ensemble.

In the above equation, $\widetilde{C}_{YD}^{n,f}$ is the $N_y \times N_n$ cross-covariance matrix between the forecast state vector and predicted data; $\widetilde{C}_{DD}^{n,f}$ is the $N_n \times N_n$ auto-covariance

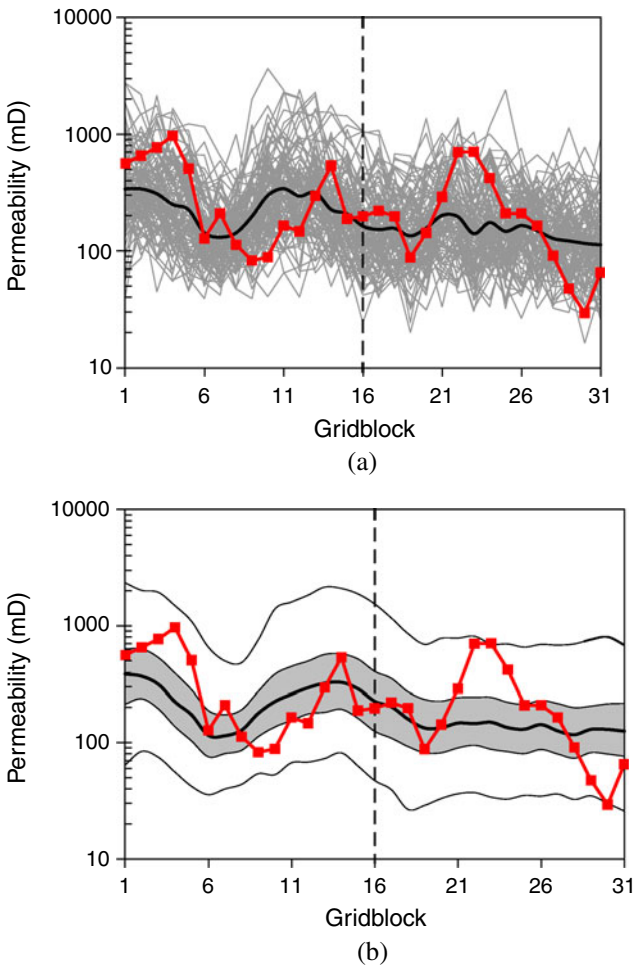

Fig. 7 Permeability after EnKF. **a** First ensemble. **b** All ensembles. The curves in this figure have the same meaning as in Fig. 5

matrix of predicted data. We introduced the tilde in $\widetilde{C}^{n,\mathrm{f}}_{\mathrm{YD}}$ and $\widetilde{C}^{n,\mathrm{f}}_{\mathrm{DD}}$ to emphasize that these matrices are estimated using the ensemble. C^n_{D} is the $N_n \times N_n$ covariance matrix of observed data measurement errors; N_n is the number of data points assimilated at the nth data assimilation time step; d^n_{uc} is a vector of "perturbed" observations, i.e., $d^n_{\mathrm{uc}} \sim \mathcal{N}(d^n_{\mathrm{obs}}, C^n_{\mathrm{D}})$ with d^n_{obs} denoting the N_n-dimensional vector of observed data at the nth data assimilation time step; and $d^{n,\mathrm{f}}$ is the corresponding vector of predicted data. The superscripts a and f denote analysis and forecast, respectively.

We assimilated data using EnKF with the ten initial ensembles of 100 models described in Section 3. Figure 7 presents the permeabilities obtained for the first ensemble and the distributions obtained by combining the ten ensembles. Compared to MCMC and RML, EnKF resulted in an unreasonably large spread in the permeability distributions. Figure 8 shows the EnKF results in terms of the predicted water production obtained by running reservoir simulations from time zero with the final ensembles. According to the results in this figure, EnKF also resulted in an unreasonably large uncertainty in W_{p} (Fig. 8a) and q_{w} (Fig. 8b).

We also observed that the distributions of W_{p} are not mutually consistent, i.e., each ensemble resulted in significantly different distributions. This particular EnKF consistency problem is well known [9, 33, 53] and is related to the dependence on the prior ensemble. In fact, each EnKF run "searches for solutions" in the specific subspace spanned by the members of the particular initial ensemble for that EnKF run.

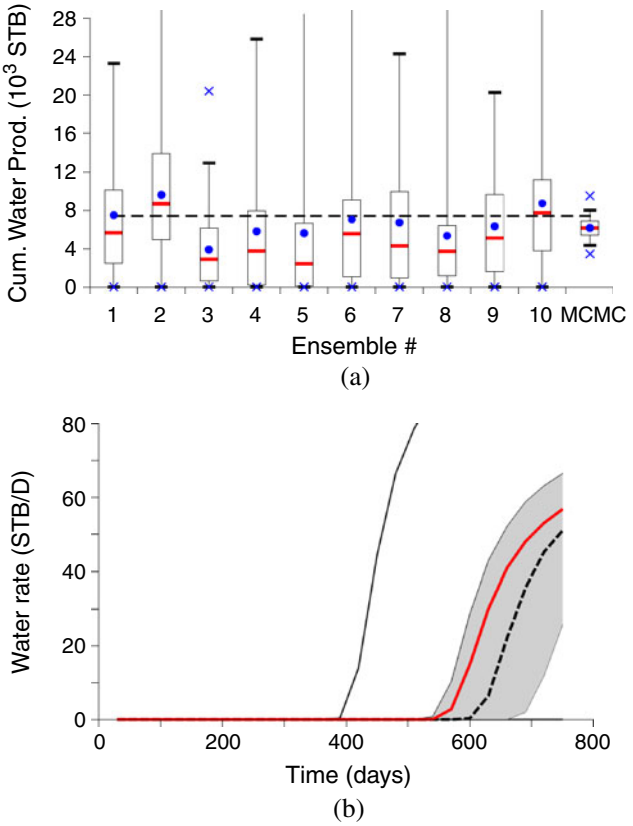

Fig. 8 Water production after EnKF. **a** Cumulative water production, W_{p}. **b** Water production rate, q_{w}. The colors in this figure have the same meaning as in Fig. 6

7 Deterministic ensemble Kalman filter

In the data assimilation literature, the ensemble-based methods are often separated into two categories: "deterministic schemes" such as the square root filters (see [48, 54] and the references therein) and

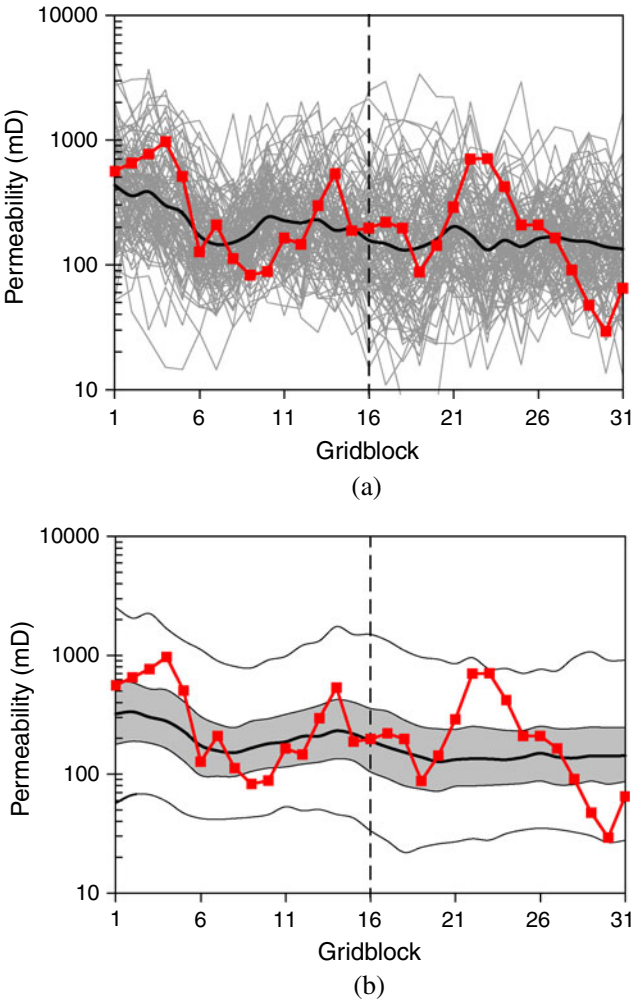

Fig. 9 Permeability after DEnKF. **a** First ensemble. **b** All ensembles. The curves in this figure have the same meaning as in Fig. 5

"perturbed-observation schemes" such as the EnKF. The main motivation for deterministic schemes is to avoid additional sampling errors caused by the process of perturbing the observations which is necessary when using the EnKF. Although deterministic schemes are very popular in the numerical weather prediction literature, these filters have seldom been used for reservoir history-matching problems. Sun et al. [50] presented a comparison of results obtained by applying four deterministic ensemble-based filters to estimate the hydraulic conductivity in two simple groundwater models. They concluded that DEnKF [47] is the most robust filter among the four studied. Thus, for the sake of brevity, we consider only DEnKF. Similar to square root filters, the DEnKF algorithm first updates the ensemble mean using the standard EnKF analysis, i.e.,

$$\overline{y}^{n,\mathrm{a}} = \overline{y}^{n,\mathrm{f}} + \widetilde{C}^{n,\mathrm{f}}_{\mathrm{YD}} \left(\widetilde{C}^{n,\mathrm{f}}_{\mathrm{DD}} + C^{n}_{\mathrm{D}} \right)^{-1} \left(d^{n}_{\mathrm{obs}} - \overline{d}^{n,\mathrm{f}} \right), \tag{13}$$

where the bar over the vectors y and d indicates the ensemble mean. The remaining terms were defined before. We define the $N_y \times N_\mathrm{e}$ matrix ΔY^n with each column corresponding to each ensemble member subtracted by the ensemble mean, i.e.,

$$\Delta Y^n = \left[y^n_1 - \overline{y}^n, \ldots, y^n_{N_\mathrm{e}} - \overline{y}^n \right]. \tag{14}$$

Then, the matrix ΔY^n is updated using

$$\Delta Y^{n,\mathrm{a}} = \Delta Y^{n,\mathrm{f}} - \frac{1}{2} \widetilde{K} \Delta D^{n,\mathrm{f}}, \tag{15}$$

where

$$\widetilde{K} = \widetilde{C}^{n,\mathrm{f}}_{\mathrm{YD}} \left(\widetilde{C}^{n,\mathrm{f}}_{\mathrm{DD}} + C^{n}_{\mathrm{D}} \right)^{-1} \tag{16}$$

is the Kalman gain and

$$\Delta D^{n,\mathrm{f}} = \left[d^{n,\mathrm{f}}_1 - \overline{d}^{n,\mathrm{f}}, \ldots, d^{n,\mathrm{f}}_{N_\mathrm{e}} - \overline{d}^{n,\mathrm{f}} \right], \tag{17}$$

is the $N_n \times N_\mathrm{e}$ matrix with columns corresponding to the predicted data obtained by each ensemble member subtracted by the mean.

We assimilated data using DEnKF and the results are presented in Figs. 9 and 10. Note that for our test problem, the overall results obtained with DEnKF are no better than those obtained with EnKF.

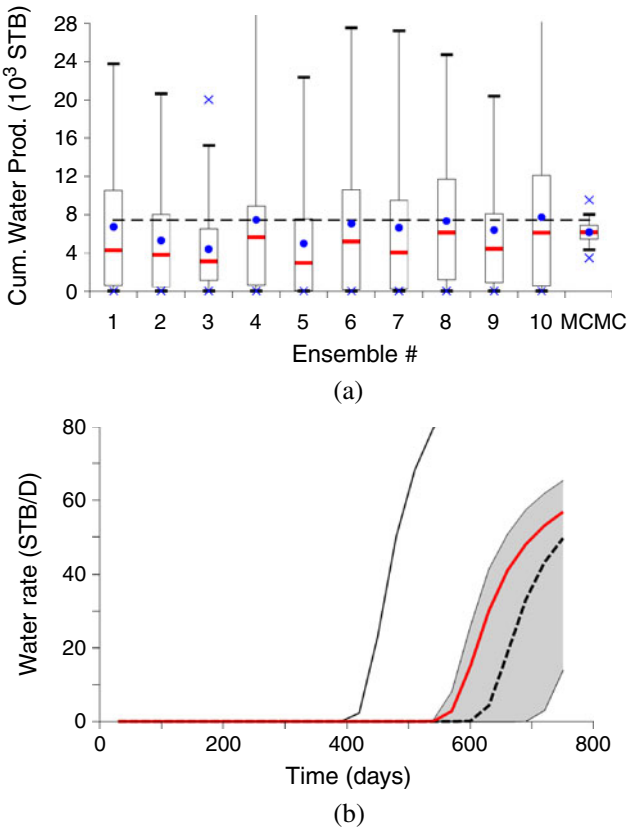

Fig. 10 Water production after DEnKF. **a** Cumulative water production, W_p. **b** Water production rate, q_w. The colors in this figure have the same meaning as in Fig. 6

8 Half-iteration EnKF

The sequential data assimilation characteristic of EnKF requires modifying the traditional history-matching problem from a parameter-estimation problem to a parameter-state-estimation problem. Specifically, when applying EnKF for history matching, it is necessary to update a combined parameter-state vector, which includes the reservoir model parameters (uncertain reservoir rock properties) and the primary variables of the reservoir simulator (typically gridblock pressure, fluid saturations, and bubble-point pressure in a standard black-oil reservoir simulator). The reason for updating primary variables, which represent the state of the dynamical system, is to avoid running the reservoir simulations from time zero after every data assimilation time step. The underlying assumption is that the updated primary variables are statistically consistent with the ones that would be obtained by running the reservoir simulator with the updated set of model parameters from time zero. However, this consistency can be proved only for problems with Gaussian statistics, a linear relation between the vector of model parameters and predicted data and negligible model error [52]. As the reservoir simulator equations are highly nonlinear, the assumption of consistency is invalid, and any significant inconsistency between model and simulator primary variables may cause a deterioration in the performance of the data assimilation [52, 56]. Moreover, the update of pressures and saturations may

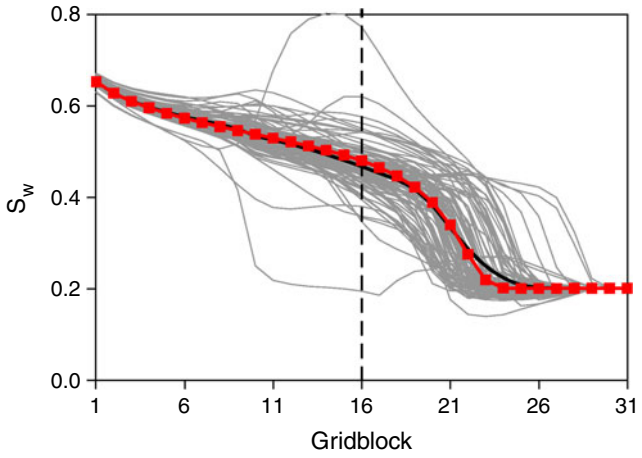

Fig. 11 Updated ensemble of water saturation at the last data assimilation time step with EnKF. The *red curve with squares* is the S_w obtained by the true model. The *solid black curve* is the ensemble mean and the *gray curves* are the ensemble members

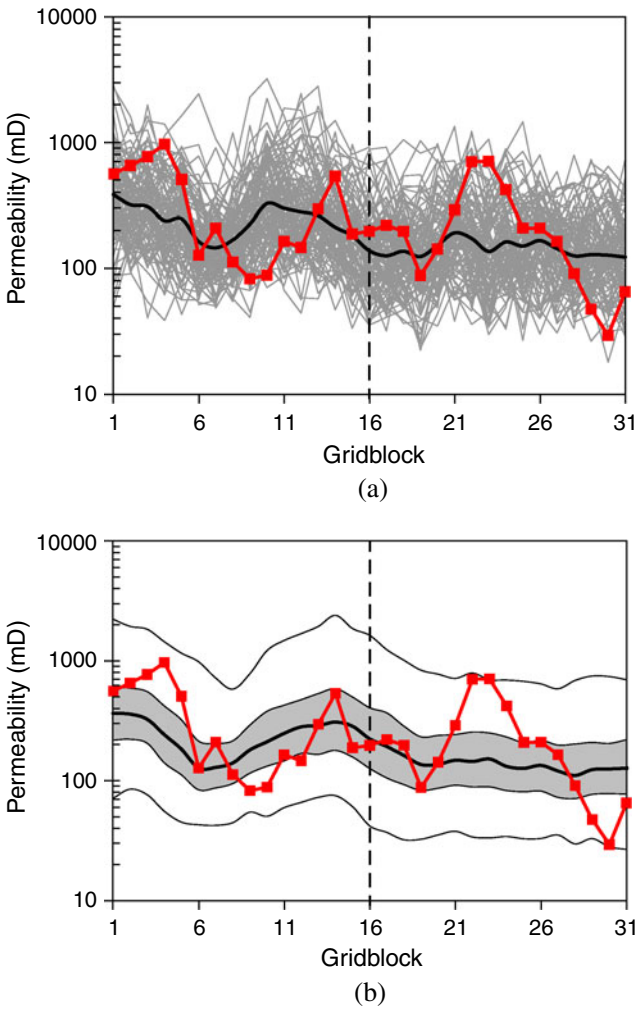

Fig. 12 Permeability after HI-EnKF. **a** First ensemble. **b** All ensembles. The curves in this figure have the same meaning as in Fig. 5

lead to nonphysical values and/or values which violate the historical material balance of the field. For example, Fig. 11 presents the analyzed ensemble of water saturation (S_w) at 360 days (last data assimilation time step) obtained from EnKF for the first of the ten ensembles considered in this paper. This figure shows that even though the mean S_w curve is in reasonable agreement with the S_w profile obtained with the true model, some ensemble members will be restarted with nonphysical values of S_w, e.g., S_w less than 0.2, which corresponds to the irreducible water saturation, and greater than 0.75, which corresponds to one minus the residual oil saturation.

Wen and Chen [57] introduced the "confirming step," which consists of rerunning the simulator starting from the previous data assimilation time step with the updated set of model parameters obtained at the current data assimilation time step in order to obtain physically plausible state variables. However, Zafari and Reynolds [59] showed that this procedure is inconsistent for the linear case, where "consistency" is defined in [52]. Perhaps, the simplest procedure to

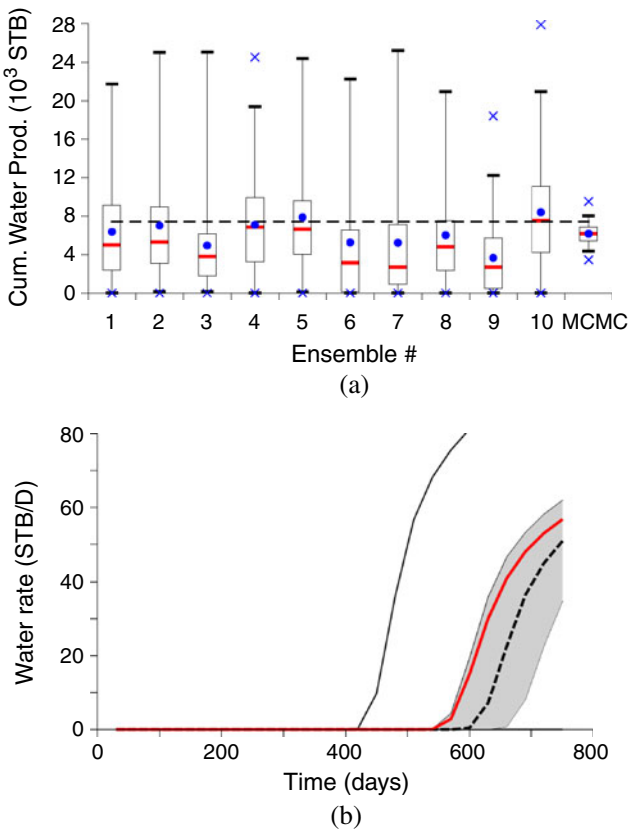

Fig. 13 Water production after HI-EnKF. **a** Cumulative water production, W_p. **b** Water production rate, q_w. The colors in this figure have the same meaning as in Fig. 6

overcome problems with inconsistency between updated model parameters and primary variables is to rerun the reservoir simulator with the latest ensemble of model parameters from time zero after each data assimilation. Wang et al. [56] refers to this procedure as half-iteration EnKF (HI-EnKF). For the example considered by [56] where both initial fluid contacts and rock property fields were updated during data assimilation, the estimates of reservoir parameters obtained with HI-EnKF were significantly better than the estimates obtained with EnKF. However, for the example considered here, the results of Figs. 12 and 13 indicate that the final history matching and uncertainty quantification results from HI-EnKF are not significantly better than those obtained with the standard EnKF. Thus, the rather poor performance of EnKF for our test problem is not primarily due to inconsistency between reservoir parameters and state variables.

9 Lorentzen–Nævdal iterative EnKF

Lorentzen and Nævdal [32] introduced an iterative procedure to improve the estimates obtained by EnKF for highly nonlinear problems. Here, we refer to this method as LN-IEnKF. The LN-IEnKF procedure used here follows:

1. At the nth data assimilation time step, update the forecast state vector, $y_j^{n,\mathrm{f}}$, using the standard EnKF equation (Eq. 12).
2. Set $\ell = 1$ and $y_j^{n,1} = y_j^{n,\mathrm{a}}$, for $j = 1, 2, \ldots, N_\mathrm{e}$.
3. Repeat
   (a) For $j = 1$ to N_e:
   - Compute the predicted data: $d_j^{n,\ell} = g(y_j^{n,\ell})$.
   - Compute $y_j^{n,\ell+1}$ using Eq. 18 (given bellow).
   - Compute $O_j^{n,\ell+1}$ using Eq. 19 (given bellow).
   - If $(O_j^{n,\ell+1} \geq O_j^{n,\ell})$ set $y_j^{n,\ell+1} = y_j^{n,\ell}$, i.e., do not update the state.

   end (for).
   (b) Set $\ell = \ell + 1$.

   until $(O_j^{n,\ell+1} \geq O_j^{n,\ell}$, for $j = 1, 2, \ldots, N_\mathrm{e})$, i.e., no states are updated; or $(\ell > 100)$, where 100 is the maximum number of iterations.

In this procedure, the state vector at the ℓth iteration is updated using

$$y_j^{n,\ell+1} = y_j^{n,\ell} + \widetilde{C}_{\mathrm{YD}}^{n,\ell} \left(\widetilde{C}_{\mathrm{DD}}^{n,\ell} + C_{\mathrm{D}}^{n} \right)^{-1} \left(d_{\mathrm{uc},j}^{n} - d_j^{n,\ell} \right), \tag{18}$$

which corresponds to the EnKF analysis (Eq. 12) with $d_j^{n,\mathrm{f}}$ replaced by $d_j^{n,\ell}$, and $\widetilde{C}_{\mathrm{YD}}^{n,\ell}$ and $\widetilde{C}_{\mathrm{DD}}^{n,\ell}$ computed based on $d_j^{n,\ell}$.

According to Lorentzen and Nævdal [32], the objective function, $O_j^{n,\ell+1}$, is evaluated using

$$\begin{aligned} O_j^{n,\ell+1} = &\left(y_j^{n,\ell+1} - y_j^{n,\mathrm{f}} \right)^{\mathrm{T}} (C_{\mathrm{Y}}^{n,\mathrm{f}})^{-1} \left(y_j^{n,\ell+1} - y_j^{n,\mathrm{f}} \right) \\ &+ \left(g(y_j^{n,\ell+1}) - d_{\mathrm{uc},j}^{n} \right)^{\mathrm{T}} (C_{\mathrm{D}}^{n})^{-1} \\ &\left(g(y_j^{n,\ell+1}) - d_{\mathrm{uc},j}^{n} \right), \end{aligned} \tag{19}$$

which corresponds to the RML objective function in terms of the state vector y_j^n. The motivation for using the RML objective function comes from the fact that the minimization of Eq. 19 for the linear case leads to the EnKF analysis equation [42]. In this equation, $(C_{\mathrm{Y}}^{n,\mathrm{f}})^{-1}$ is the inverse of the forecast state covariance matrix, which is fixed during the iterations. Lorentzen and Nævdal [32] do not mention how they compute $(C_{\mathrm{Y}}^{n,\mathrm{f}})^{-1}$. Here, we approximate $C_{\mathrm{Y}}^{n,\mathrm{f}}$ based on the forecast ensemble and compute its inverse using singular value decomposition (SVD).

The LN-IEnKF method requires one to compute the predicted data vector, $d_j^{n,\ell}$, for a given updated state vector, $y_j^{n,\ell}$, i.e., $d_j^{n,\ell} = g(y_j^{n,\ell})$. For a typical reservoir history-matching problem, the observations correspond to data at wells, e.g., well water-cut or bottomhole pressure data. In this case, $g(y_j^{n,\ell})$ can be computed using Peaceman's equation [40]. However, for the test case considered in this paper, the observations correspond to the pressure at the 16th gridblock. Hence, $d_j^{n,\ell} = g(y_j^{n,\ell})$ is simply an entry of the vector $y_j^{n,\ell}$.

Figures 14 and 15 present the results obtained after data assimilation with LN-IEnKF. These figures show that LN-IEnKF did not improve the results obtained with the standard EnKF. The failure of LN-IEnKF to improve results can be explained as follows: (1) the first step of the LN-IEnKF method is the analysis of the forecast state vector using the standard EnKF, (2) the predicted data correspond to a component of the state vector $y_j^{n,\ell}$, and (3) the measurement errors are small so

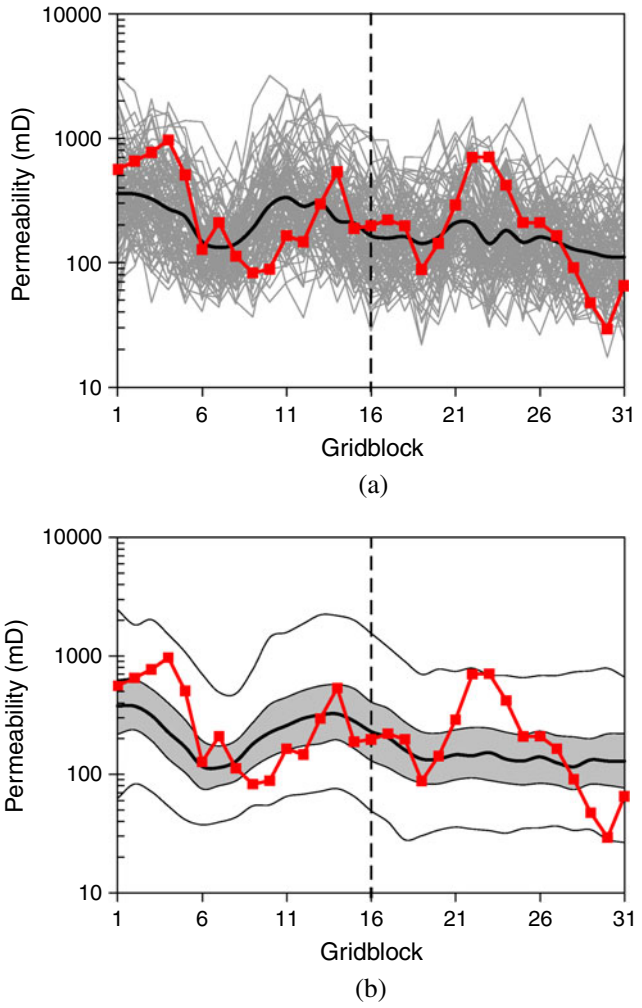

Fig. 14 Permeability after LN-IEnKF. **a** First ensemble. **b** All ensembles. The curves in this figure have the same meaning as in Fig. 5

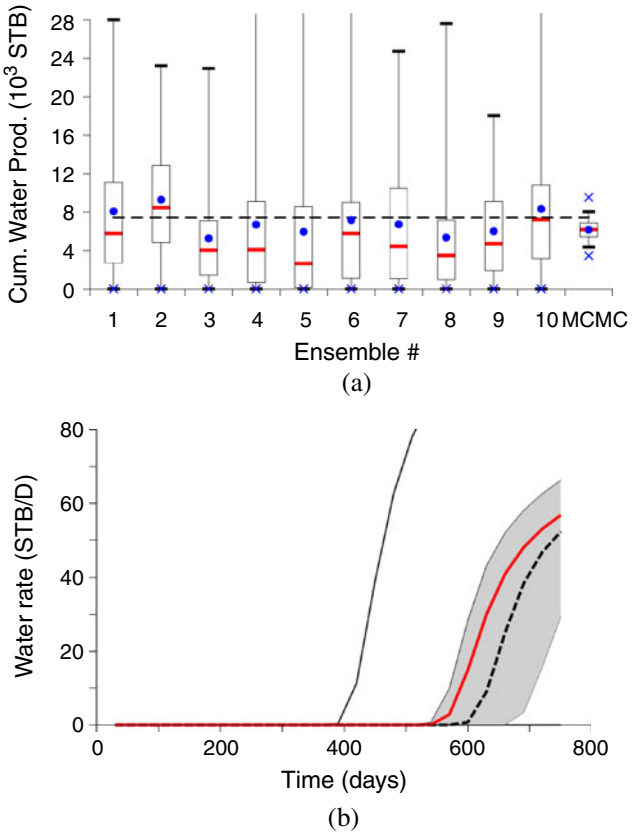

Fig. 15 Water production after LN-IEnKF. **a** Cumulative water production, W_p. **b** Water production rate, q_w. The colors in this figure have the same meaning as in Fig. 6

that $\widetilde{C}_{DD}^{n,f} + C_D^n \approx \widetilde{C}_{DD}^{n,f}$. In this case, it is straightforward to show that after EnKF analysis, we have

$$\begin{aligned} d_j^{n,a} &= d_j^{n,f} + \widetilde{C}_{DD}^{n,f}\left(\widetilde{C}_{DD}^{n,f} + C_D^n\right)^{-1}\left(d_{uc,j}^n - d_j^{n,f}\right) \\ &\approx d_j^{n,f} + \widetilde{C}_{DD}^{n,f}\left(\widetilde{C}_{DD}^{n,f}\right)^{-1}\left(d_{uc,j}^n - d_j^{n,f}\right) \\ &\approx d_{uc,j}^n \end{aligned} \tag{20}$$

provided that $\widetilde{C}_{DD}^{n,f}$ is nonsingular, which is true for the test case because $\widetilde{C}_{DD}^{n,f}$ is a 1×1 nonzero matrix at each data assimilation time step. Hence, at the first iteration of LN-IEnKF, we have $d_j^{n,1} = g(y_j^{n,a}) = d_j^{n,a} \approx d_{uc,j}^n$. This makes the subsequent updates with Eq. 18 very small because $d_{uc,j}^n - d_j^{n,\ell} \approx 0$. Consequently, LN-IEnKF gives results close to those obtained with EnKF.

10 Krymskaya–Hanea–Verlaan iterative EnKF

Krymskaya et al. [24] also proposed an iterative form of EnKF for reservoir history-matching problems. Here, we refer to this method as KHV-IEnKF. In this method, we assimilate data with standard EnKF and use the final ensemble mean of the vectors of model parameters as the "prior mean" for a subsequent data assimilation. The KHV-IEnKF procedure used here follows:

1. Initialize $\overline{m}^0 = m_{pr}$ and $\ell = 0$.
2. Generate the ensemble of model parameters by sampling $m_j^\ell \sim \mathcal{N}(\overline{m}^\ell, C_M)$, for $j = 1, 2, \cdots, N_e$.
3. Assimilate data using EnKF and set $m_j^{\ell+1} = m_j^a$, for $j = 1, 2, \cdots, N_e$, where m_j^a is the analyzed vector of model parameters.

4. Rerun the ensemble from time zero and compute the average objective function:

$$\overline{O}^{\ell+1} = \frac{1}{N_e}\sum_{j=1}^{N_e} O\left(m_j^{\ell+1}\right),$$

where $O(m_j^{\ell+1})$ is computed using Eq. 2.

5. If $\left(\left|\frac{\overline{O}^{\ell+1}-\overline{O}^{\ell}}{\overline{O}^{\ell}+10^{-8}}\right| < 10^{-3}\right)$ or $(\ell = 10)$, then:
   - Stop data assimilation.

   Else,
   - Compute the ensemble mean:

$$\overline{m}^{\ell+1} = \frac{1}{N_e}\sum_{j=1}^{N_e} m_j^{\ell+1}.$$

   - Set $\ell = \ell + 1$.
   - Return to step 2.

   end (if).

In the above procedure, we chose the maximum number of iterations equal to ten. In [24], the authors use the "confirming step" [57] procedure to avoid non-physical values of pressure and fluids saturation when restarting the reservoir simulations, but as mentioned previously, this procedure is inconsistent for the linear-Gaussian case [59] so it is not used here. Unfortunately, the KHV-IEnKF is also inconsistent for the linear-Gaussian case. By simple inspection of the algorithm, we can conclude that KHV-IEnKF will not provide a correct sampling of the posterior PDF for the linear-Gaussian case because we use the posterior mean from the previous iteration as the prior mean for the next iteration, which is clearly statistically incorrect. Nevertheless, we assimilate data using KHV-IEnKF.

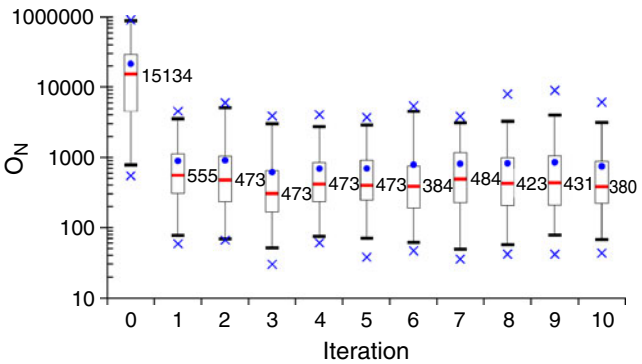

Fig. 16 Box plots of the normalized objective function after each iteration of KHV-IEnKF (first ensemble). The *numbers* next to the boxes correspond to the median of O_N

Figure 16 presents the box plots of O_N after each of the ten iterations where the first iteration of KHV-IEnKF is identical to EnKF. The results show that the KHV-IEnKF data match is only slightly better than the EnKF data match; also note that O_N is not a monotonically decreasing function of the iteration number.

Figure 17a presents the permeability obtained with KHV-IEnKF for the first of the ten ensembles. This figure shows that the mean permeability is overly rough, indicating possible overcorrections to the permeability field caused by the iterations. Figure 17b presents the permeability distribution obtained by combining the ten ensembles. As shown, the KHV-IEnKF results in a distribution very different from the reference distribution obtained with MCMC. Figure 18 shows that distributions of predicted water production generated with KHV-IEnKF results in a large overestimation of uncertainty in the predicted water rate.

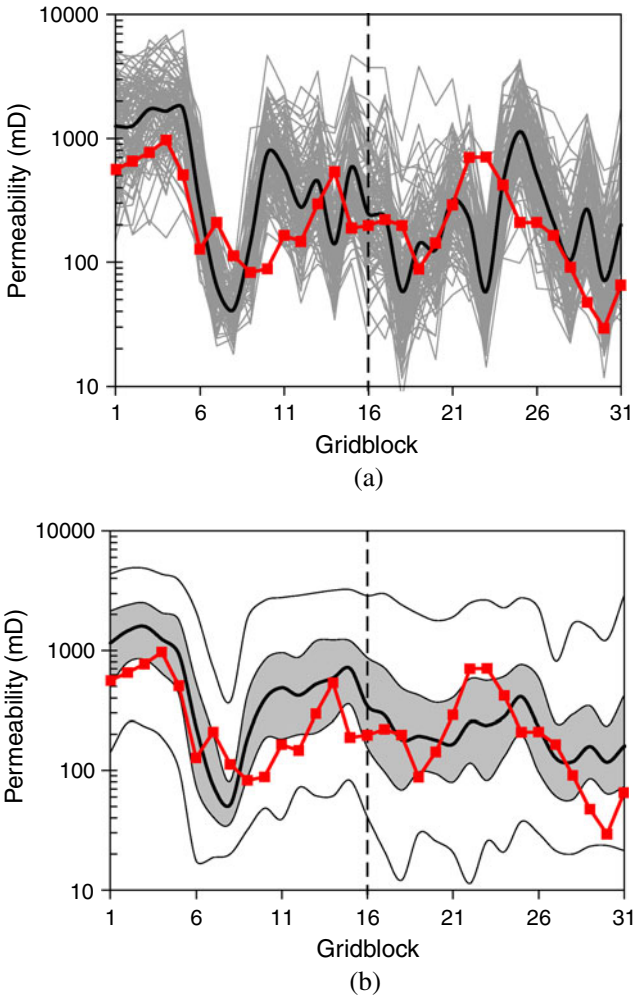

Fig. 17 Permeability after KHV-IEnKF. **a** First ensemble. **b** All ensembles. The curves in this figure have the same meaning as in Fig. 5

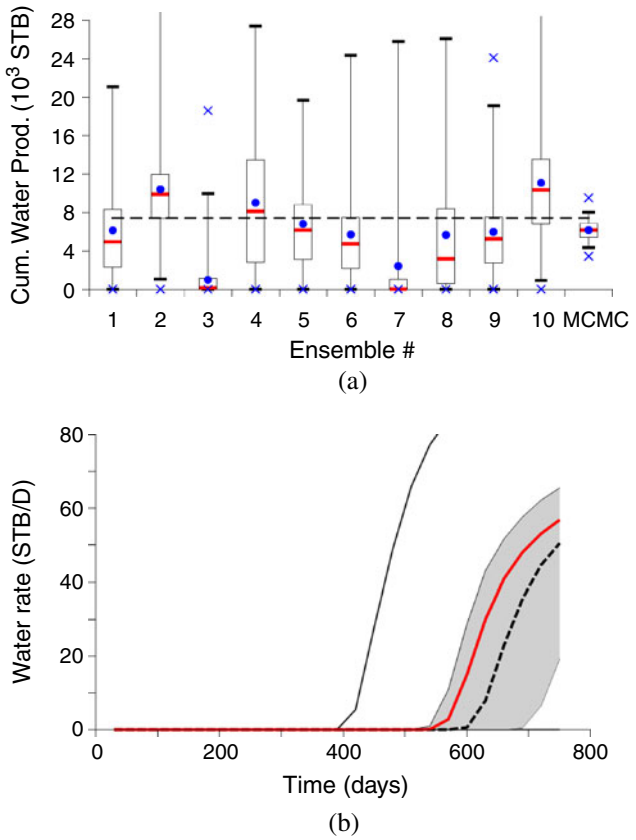

Fig. 18 Water production after KHV-IEnKF. **a** Cumulative water production, W_p. **b** Water production rate, q_w. The colors in this figure have the same meaning as in Fig. 6

11 EnKF-MCMC

EnKF-MCMC was proposed by Emerick and Reynolds [9] as an approximate method to improve the sampling results of EnKF. In this method, we first assimilate data with EnKF. Then, we use the final ensemble to propose transitions for a MCMC procedure. During MCMC, we avoid reservoir simulations by proposing a combined parameter-state vector, $\widehat{y}$, which is used to approximate the likelihood part of the posterior PDF. Specifically, after data assimilation with EnKF, we run the resulting ensemble from time zero and build the matrix

$$\Delta Y = Y - \overline{Y} = \begin{bmatrix} \Delta M \\ \Delta P^1 \\ \Delta P^2 \\ \vdots \\ \Delta P^{N_t} \end{bmatrix}. \tag{21}$$

Here, $\Delta M = M - \overline{M}$, where M is the $N_m \times N_e$ matrix with the jth column equal to the jth realization of the vector of model parameters obtained by data assimilation with EnKF and $\overline{M}$ is the $N_m \times N_e$ matrix with all columns equal to $\overline{m}$, which represents the average of all columns of M, i.e., the ensemble mean. Similarly, $\Delta P^n = P^n - \overline{P}^n$, where P^n is the $N_p \times N_e$ matrix with its jth column equal to the jth vector of reservoir simulator primary variables at the nth data assimilation time step. Each column of $\overline{P}^n$ is equal to $\overline{p}^n$, the average of the columns of P^n. N_t denotes the total number of data assimilation time steps. In [9], we included in Y the primary variables required to compute well data with Peaceman's equation [40]. Here, because our observations correspond to the pressure at the gridblock of the monitor well, we do not need to use Peaceman's equation. In fact, the only primary variables we need to include in Y are the predicted pressures at the 16th gridblock for the 12 data assimilation time steps. After building the matrix ΔY, we apply SVD and approximate the square root of the covariance of the state vector using

$$\widetilde{C}_Y^{1/2} = \frac{U_r \Lambda_r U_r^T}{\sqrt{N_e - 1}}, \tag{22}$$

where U_r is the $N_y \times N_r$ matrix with the left singular vectors of ΔY corresponding to the nonzero singular values and Λ_r is the $N_r \times N_r$ diagonal matrix containing the nonzero singular values ΔY. $N_r = \min\{N_y, N_e - 1\}$. We use $\widetilde{C}_Y^{1/2}$ to propose states in the Markov chain with local perturbations using

$$\widehat{y} = y + \widetilde{C}_Y^{1/2} \delta z, \tag{23}$$

where y is the current state in the chain and δz is a sample from $\mathcal{N}(0, \sigma^2 I_{N_y})$. Besides gridblock log-permeabilities, $\widehat{y}$ contains the estimated values of pressure at the gridblock containing the monitor well for the 12 data assimilation time steps. These values of gridblock pressure are used as predicted data to compute the objective function (Eq. 2) required to evaluate the acceptance probability in the Metropolis–Hastings algorithm. With this procedure, we propose states for Markov chains without reservoir simulation runs. However, because the acceptance probability is based on an approximate likelihood, MCMC will not exactly sample the posterior PDF. Because of this, Emerick and Reynolds [9] applied EnKF-MCMC iteratively, where the final ensemble after MCMC is used to propose states for new Markov chains. The EnKF-MCMC algorithm used here can be summarized as follows:

1. Perform data assimilation using EnKF.
2. For $\ell = 1$ to 10 (where 10 is the total number of iterations):
   (a) Run the ensemble from time zero.

(b) Build the matrix ΔY (Eq. 21) and compute the matrices U_r and Λ_r using SVD. These matrices are used to estimate $\widetilde{C}_Y^{1/2}$ (Eq. 22).

(c) Build $N_e = 100$ Markov chains to generate the new ensemble. For each Markov chain:
- Start the jth chain with the jth model of the ensemble at the previous iteration.
- Propose 5,000 states using local perturbations (Eq. 23) with $\sigma = 0.05$.
- Keep the last accepted state as one sample.

end (for).

The setup of the Markov chains with 5,000 proposals and $\sigma = 0.05$ was obtained from a small number of experiments. The objective is to run each chain long enough to pass through the transitional (burn-in) period and choose a single model as a sample. Figure 19 presents the box plots of O_N after each of the ten iterations of EnKF-MCMC. This figure indicates that O_N is a continuously decreasing function of the iteration number, but after five iterations, the rate of decrease is very slow.

In [9], we applied EnKF-MCMC with ten different initial ensembles and resampled the final models based on the value of O_N. In this procedure, we compute an important weight for each model using

$$w_j = \frac{\exp(-O_N(m_j))}{\sum_{k=1}^{N_s} \exp(-O_N(m_k))}, \text{ for } j = 1, 2, \cdots, N_s, \quad (24)$$

where N_s is the total number of samples resulting from the multiple EnKF-MCMC runs. Here, $N_s = 10 \times 100 = 1{,}000$. Figure 20 presents the permeabilities obtained for the first of the ten initial ensembles after EnKF-MCMC (Fig. 20a) and the permeability distributions obtained by combining the ten ensembles before (Fig. 20b) and after (Fig. 20c) resampling with Eq. 24. Compared to MCMC, the spreads in the permeability distributions obtained with EnKF-MCMC

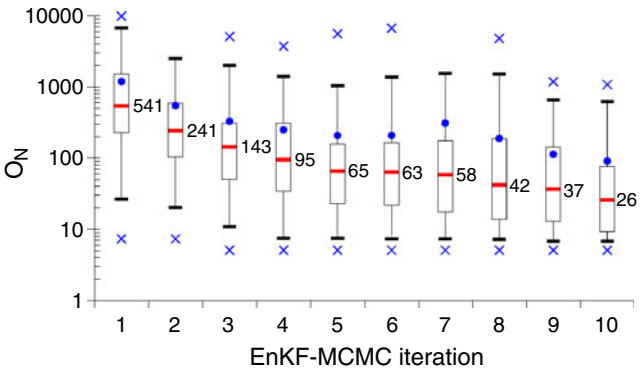

Fig. 19 Box plots of the normalized objective function after each iteration of EnKF-MCMC (first ensemble). The *numbers* next to the boxes correspond to the median of O_N

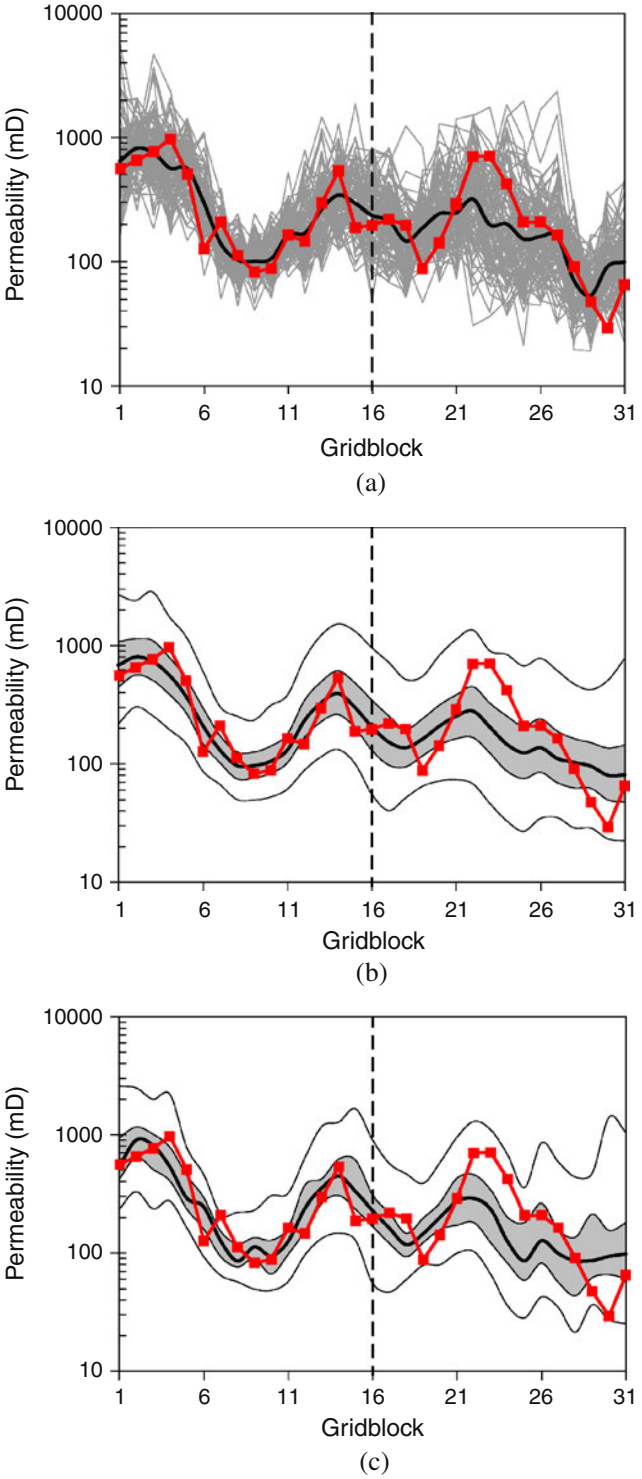

Fig. 20 Permeability after EnKF-MCMC. **a** First ensemble (no resampling). **b** All ensembles (no resampling). **c** All ensembles (after resampling). The curves in this figure have the same meaning as in Fig. 5

are slightly overestimated although the results can be considered acceptable. Resampling based on O_N did not change appreciably the permeability distributions. Figure 21 shows the results in terms of water production. Figure 21a shows that each ensemble resulted in significantly different distributions of W_p, and the variance of each distribution is overestimated compared to MCMC. Figure 21b shows that before resampling, EnKF-MCMC greatly overestimates the uncertainty in the predicted water production. After resampling (Fig. 21c), the distribution of q_w is in reasonable agreement with MCMC although some overestimation of the spread is still observed.

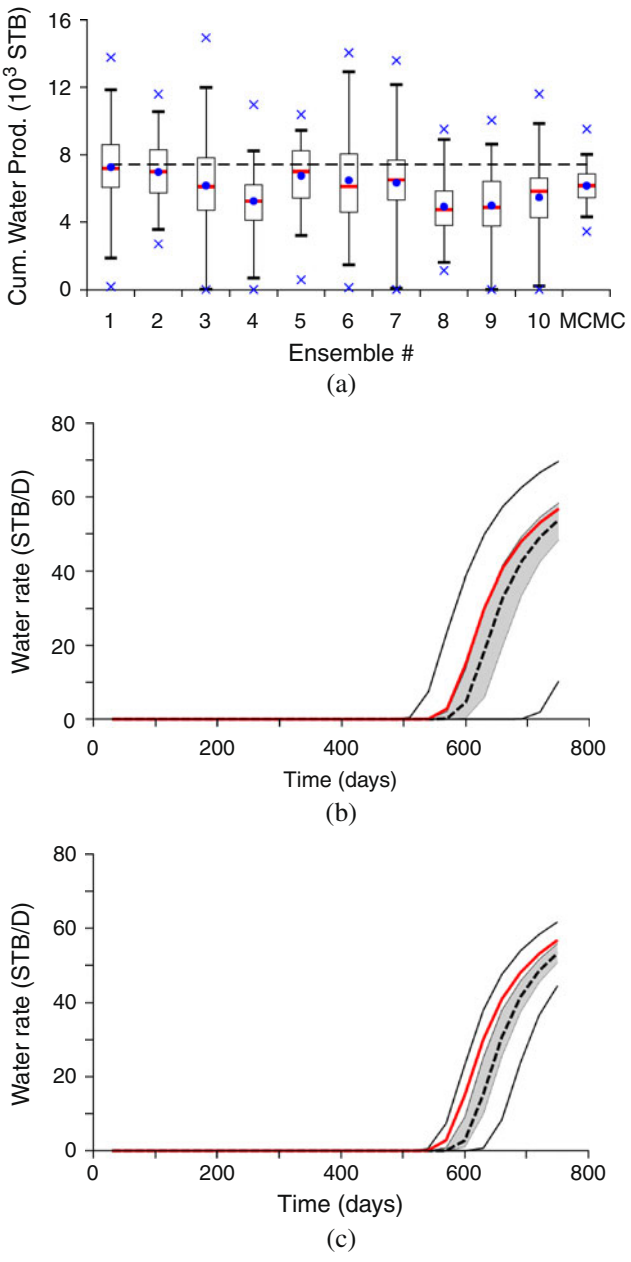

Fig. 21 Water production after EnKF-MCMC. **a** Cumulative water production, W_p, (no resampling). **b** Water production rate, q_w (no resampling). **c** Water production rate, q_w (after resampling). The colors in this figure have the same meaning as in Fig. 6

12 Ensemble smoother

ES was introduced by van Leeuwen and Evensen [55]. Unlike EnKF, ES does not assimilate data sequentially in time. Instead, ES computes a global update including all data available. Other than that, the ES formulation is similar to EnKF. For ES, we write the analyzed vector of model parameters, m^a, as

$$m_j^a = m_j^f + \widetilde{C}_{MD}^f \left(\widetilde{C}_{DD}^f + C_D\right)^{-1} \left(d_{uc,j} - d_j^f\right), \qquad (25)$$

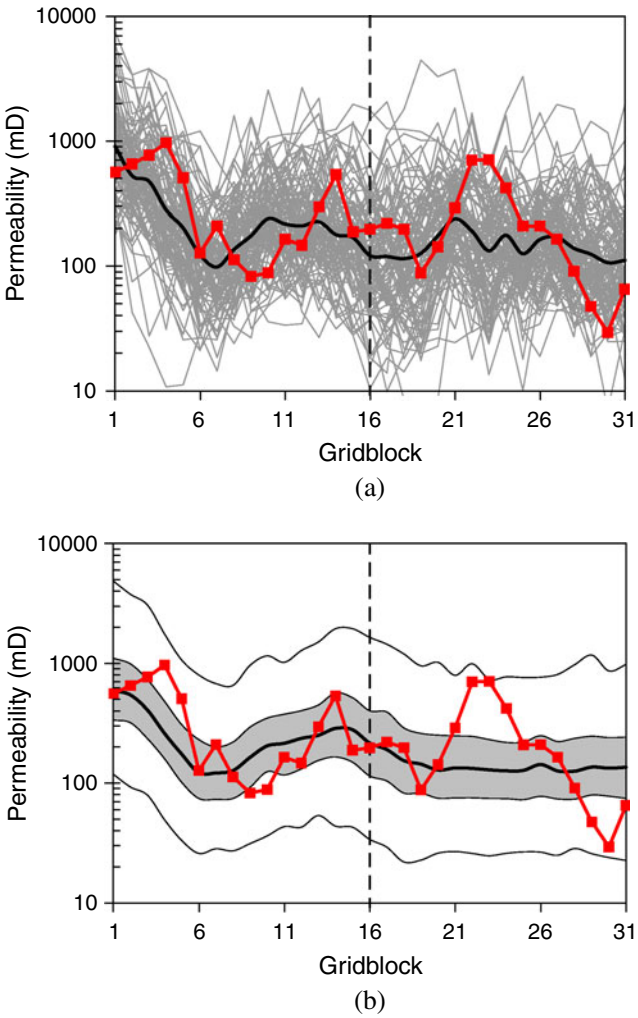

Fig. 22 Permeability after ES. **a** First ensemble. **b** All ensembles. The curves in this figure have the same meaning as in Fig. 5

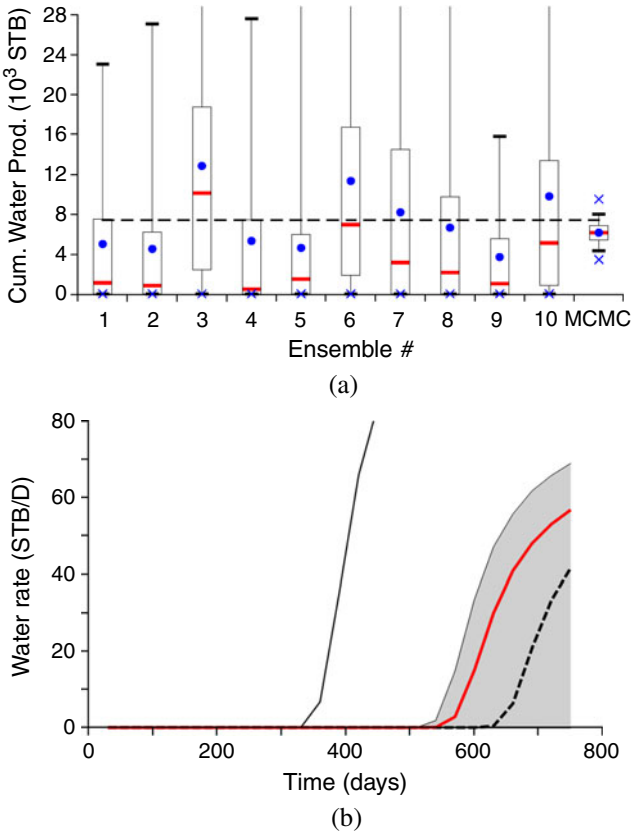

Fig. 23 Water production after ES. **a** Cumulative water production, W_p. **b** Water production rate, q_w. The colors in this figure have the same meaning as in Fig. 6

for $j = 1, 2, \cdots, N_e$. The notation is similar to the one used for EnKF. $\widetilde{C}^f_{MD}$ is the cross-covariance matrix between the prior vector of model parameters, m^f, and the vector of predicted data, d^f; $\widetilde{C}^f_{DD}$ is the $N_d \times N_d$ auto-covariance matrix of predicted data; and d_{uc} and C_D were defined before when we presented the RML method. Note that, because we assimilate all data simultaneously, there is no need to restart reservoir simulations in ES. For this reason, we wrote Eq. 25 only in terms of the vector of model parameters.

Figures 22 and 23 present the results obtained after data assimilation with ES. For ES, the conclusions are essentially the same as the ones obtained for EnKF, i.e., a large overestimation of uncertainty and inconsistent distributions of W_p. In fact, the overestimation of uncertainty with ES is greater than with EnKF.

13 Ensemble smoother with multiple data assimilation

Reynolds et al. [42] showed that EnKF is equivalent to applying the first iteration of the Gauss–Newton method sequentially, with a full step and replacing the sensitivity matrix by an ensemble-average sensitivity matrix. This means that, for ES, a single Gauss–Newton correction is applied for conditioning the ensemble to all data available. Therefore, ES may not be able to provide reasonable data matches when applied to reservoir problems.

Emerick and Reynolds [10] introduced a procedure to improve the data matches obtained with ES based on assimilating the same data multiple times with an inflated covariance matrix of the measurement errors. This method is motivated by the equivalence between single and multiple data assimilations for the linear-Gaussian case as shown in [10, 11]. This procedure can be interpreted as an iterative ES, where the number of "iterations" must be selected a priori. The ES-MDA method can be summarized as follows:

1. Choose the number of data assimilations, N_a, and the multiplication coefficients of the data covariance matrix, α_i, for $i = 1, 2, \ldots, N_a$.
2. For $i = 1$ to N_a:
   (a) Run the ensemble from time zero.
   (b) For each ensemble member, perturb the observation vector using $d_{uc} = d_{obs} + \sqrt{\alpha_i} C_D^{1/2} z_d$, where $z_d \sim \mathcal{N}(0, I_{N_d})$.
   (c) Update the ensemble using Eq. 25 with C_D replaced by $\alpha_i C_D$.

   end (for).

The α_i coefficients must be selected such that

$$\sum_{i=1}^{N_a} \frac{1}{\alpha_i} = 1. \tag{26}$$

The simplest choice for the α_i coefficients in $\alpha_i = N_a$ for $i = 1, 2, \ldots, N_a$. However, the results in [10] indicate that choosing α_i values in a decreasing order

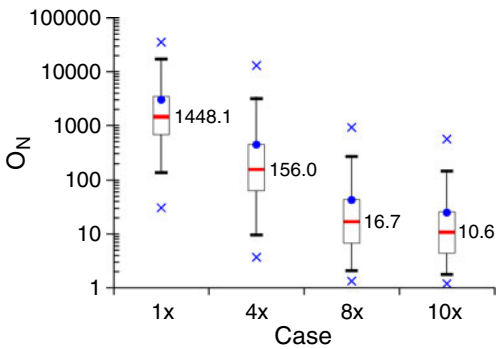

Fig. 24 Box plots of the normalized objective function for ES-MDA. The *numbers* next to the boxes correspond to the median of O_N

may improve the data assimilation. The rationale is to apply smaller corrections in the ensemble for the early iterations by choosing large α_i values and decrease α_i gradually. Figure 24 presents the box plots of O_N for ES with one, four, eight, and ten data assimilations. In these results, the following values of the α_i coefficients were used:

- $4\times$: $\alpha_1 = 9.333$, $\alpha_2 = 7.0$, $\alpha_3 = 4.0$, and $\alpha_4 = 2.0$.
- $8\times$: $\alpha_1 = 20.719$, $\alpha_2 = 19.0$, $\alpha_3 = 17.0$, $\alpha_4 = 16.0$, $\alpha_5 = 15.0$, $\alpha_6 = 9.0$, $\alpha_7 = 5.0$, and $\alpha_8 = 2.5$.
- $10\times$: $\alpha_1 = 57.017$, $\alpha_2 = 35.0$, $\alpha_3 = 25.0$, $\alpha_4 = 20.0$, $\alpha_5 = 18.0$, $\alpha_6 = 15.0$, $\alpha_7 = 12.0$, $\alpha_8 = 8.0$, $\alpha_9 = 5.0$, and $\alpha_{10} = 3.0$.

These coefficients were chosen based on our experience with other synthetic reservoir cases [10]. We have experimented with different coefficients, but we did not obtain any results significantly different from those shown here. According to the results in Fig. 24, after ten data assimilations, the median of O_N is reduced from 1,448 to 10.6. Figure 25 presents the permeabilities obtained by ES-MDA ($10\times$). Unlike EnKF and ES, ES-MDA results in a fairly low spread of permeabilities, which are in reasonable agreement with the MCMC results. In terms of W_p (Fig. 26a), each ES-MDA ($10\times$) ensemble results in distributions with roughly the same variance obtained from MCMC. However, there is still variation between the distributions obtained for different ensembles; compare, for example, the box plots for the fourth and seventh ensembles in Fig. 26a. This means that a single ensemble is not enough to obtain a reliable quantification of uncertainty. However, combining the results of the ten ensembles (Fig. 26b) results in a distribution of q_w that is very close to the one obtained with MCMC.

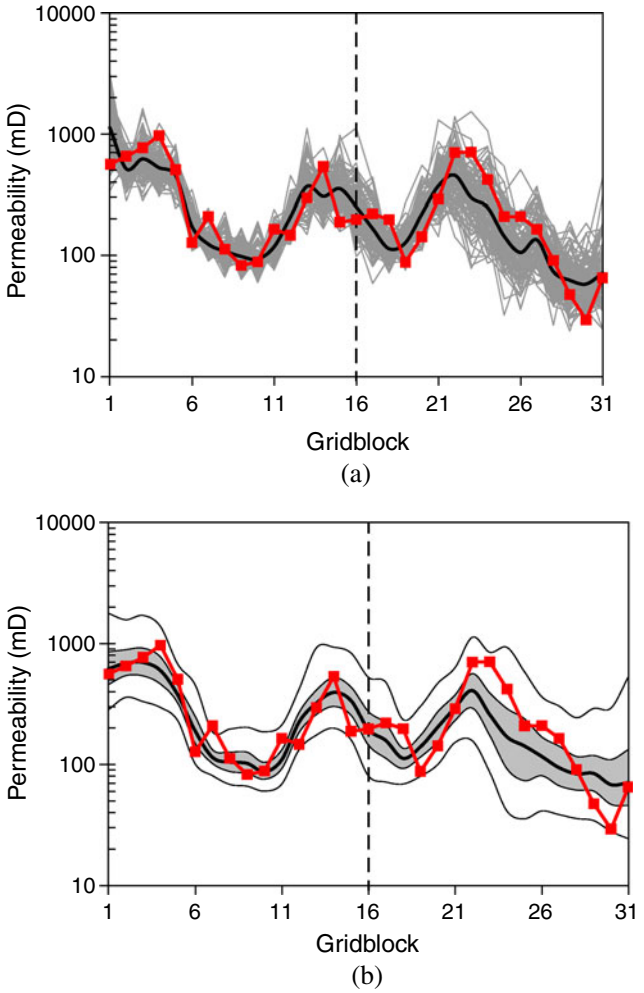

Fig. 25 Permeability after ES-MDA ($10\times$). **a** First ensemble. **b** All ensembles. The curves in this figure have the same meaning as in Fig. 5

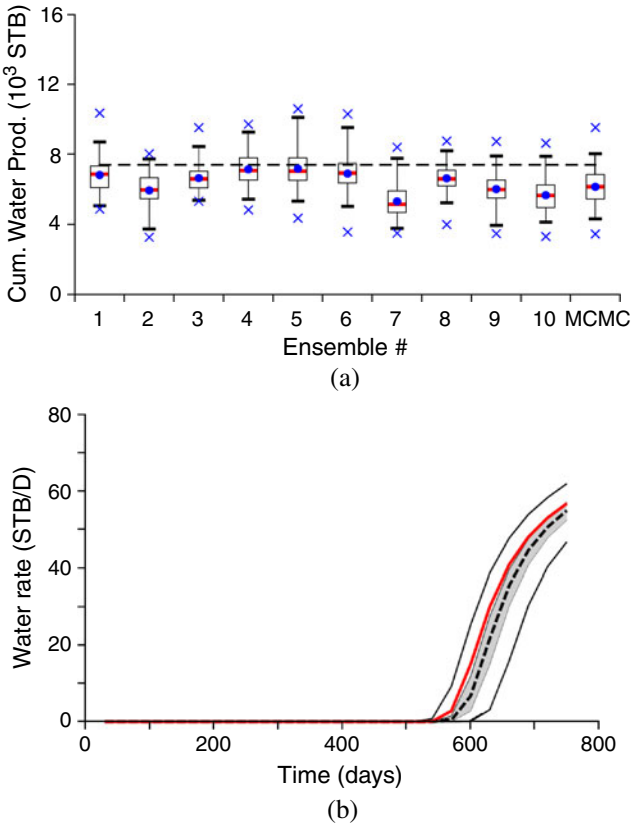

Fig. 26 Water production after ES-MDA. **a** Cumulative water production. **b** Water production rate. The colors in this figure have the same meaning as in Fig. 6

14 EnRML

EnRML was introduced by Gu and Oliver [18] as an iterative EnKF. EnRML uses a Gauss–Newton update

equation with an "average sensitivity matrix" estimated from the ensemble. EnRML updates the ensemble using

$$m_j^{\ell+1} = m_j^{\ell} + \beta_\ell \delta m_j^{\ell+1}, \text{ for } j = 1, 2, \cdots, N_e, \tag{27}$$

with

$$\delta m_j^{\ell+1} = m_j^{\mathrm{f}} - m_j^{\ell} - \widetilde{C}_{\mathrm{M}}^{\mathrm{f}} \widetilde{G}_\ell^{\mathrm{T}} \left(\widetilde{G}_\ell \widetilde{C}_{\mathrm{M}}^{\mathrm{f}} \widetilde{G}_\ell^{\mathrm{T}} + C_{\mathrm{D}} \right)^{-1} \times \left[d_j^{\ell} - d_{\mathrm{uc},j} - \widetilde{G}_\ell \left(m_j^{\ell} - m_j^{\mathrm{f}} \right) \right]. \tag{28}$$

In the above equations, ℓ denotes the iteration index and β_ℓ denotes the step size. During the iterative process, $\widetilde{C}_{\mathrm{M}}^{\mathrm{f}}$ is fixed and estimated based on the forecast ensemble. The average sensitivity matrix, $\widetilde{G}$, is computed using

$$\widetilde{G}_\ell = \Delta D^\ell \left(\Delta M^\ell \right)^+, \tag{29}$$

where the superscript "+" denotes the pseudo-inverse of ΔM^ℓ computed by SVD. $\Delta D^\ell = D^\ell - \overline{D}^\ell$, where D^ℓ is the matrix with the ensemble of predicted data at the ℓth iteration, i.e., the jth column of D^ℓ corresponds to the predicted data from the jth ensemble member. $\overline{D}^\ell$ is the matrix with all columns equal to $\overline{d}^\ell$, which represents the average of all columns of D^ℓ. Similarly, $\Delta M^\ell = M^\ell - \overline{M}^\ell$, where the jth column of M^ℓ contains the vector of model parameters corresponding to the jth ensemble member at the ℓth iteration. $\overline{M}^\ell$ is the matrix with all columns equal to $\overline{m}^\ell$, which represents the average of all columns of M^ℓ.

In the original EnRML method, data are assimilated sequentially in time. Here, we refer to this method as EnRML-F, where "F" stands for filter. [7] proposed to use EnRML as a smoother, in which case, all data are assimilated simultaneously. We refer to this procedure as EnRML-S. Unfortunately, Gu and Oliver [18] do not provide details on how they choose or manage β_ℓ. Here, we use the following implementation of EnRML:

1. Run the ensemble from time zero until the next data assimilation time step (EnRML-F) or until the end of the history (EnRML-S).
2. Initialize: $\ell = 0$, $\beta_0 = 1$, and $m_j^0 = m_j^{\mathrm{f}}$ for $j = 1, 2, \ldots, N_e$.
3. Compute $\widetilde{G}_\ell$ (Eq. 29).
4. For $j = 1$ to N_e:
   (a) Compute $m_j^{\ell+1}$ (Eqs. 27 and 28).
   (b) Rerun ensemble from time zero.
   (c) Compute $O_{d,j}^{\ell+1} = 0.5 \left(d_j^{\ell+1} - d_{\mathrm{uc},j} \right)^{\mathrm{T}} C_{\mathrm{D}}^{-1} \left(d_j^{\ell+1} - d_{\mathrm{uc},j} \right)$.

   end (for).
5. Compute $\overline{O}_d^{\ell+1} = \frac{1}{N_e} \sum_{j=1}^{N_e} O_{d,j}^{\ell+1}$.
6. If $\overline{O}_d^{\ell+1} < \overline{O}_d^{\ell}$, then:
   (a) Accept the step and increase the step size for the next iteration, $\beta_{\ell+1} = 2\beta_\ell$.
   (b) If $\beta_{\ell+1} > \beta_0$, then set $\beta_{\ell+1} = \beta_0$.
   (c) Increase the iteration index, $\ell = \ell + 1$.

   Else:
   (a) Reduce the step size, $\beta_\ell = \beta_\ell / 2$.
   (b) Return to step 4.

   end (if).
7. Check termination criteria.
8. If any one of the termination criteria is satisfied, then go to the next data assimilation time step (EnRML-F) or stop the data assimilation (EnRML-S). Otherwise, return to step 3.

We use the following termination criteria:

- $\max |m_{i,j}^{\ell+1} - m_{i,j}^{\ell}| < 10^{-5}$ for $i = 1, 2, \ldots, N_m$ and $j = 1, 2, \ldots, N_e$.
- $\left| \frac{\overline{O}_d^{\ell+1} - \overline{O}_d^{\ell}}{\overline{O}_d^{\ell}} \right| < 10^{-4}$.
- Maximum number of iterations = 10.
- Maximum number of step size cuts = 5.

The first two termination criteria were chosen as the same as used in [18].

The estimate $\widetilde{G}$ of the sensitivity matrix is clearly the main approximation introduced in the EnRML method. Figure 27 presents the values of $\widetilde{G}$ calculated for the first of the ten initial ensembles and the actual sensitivity matrix, G, computed using the adjoint method evaluated at the prior mean. According to Fig. 27, $\widetilde{G}$ is very noisy. However, if we consider the product $\widetilde{C}_{\mathrm{M}}^{\mathrm{f}} \widetilde{G}^{\mathrm{T}}$ (Fig. 28), we observe a smoother behavior and a qualitative agreement with the actual product, $C_{\mathrm{M}} G^{\mathrm{T}}$, computed with the adjoint method. Note that, for EnRML, we computed $\widetilde{C}_{\mathrm{M}}^{\mathrm{f}} \widetilde{G}^{\mathrm{T}}$ using the ensemble approximation for $C_{\mathrm{M}}^{\mathrm{f}}$, while for the adjoint case, we used the correct prior covariance matrix C_{M}. Figures 27 and 28 illustrate that while the $\widetilde{G}$ estimated from EnRML using Eq. 29 is highly inaccurate, the resulting product $\widetilde{C}_{\mathrm{M}}^{\mathrm{f}} \widetilde{G}^{\mathrm{T}}$ is reasonably similar to the true $C_{\mathrm{M}} G^{\mathrm{T}}$. In particular, each entry of $\widetilde{C}_{\mathrm{M}}^{\mathrm{f}} \widetilde{G}^{\mathrm{T}}$ has the same sign as the corresponding entries of the true $C_{\mathrm{M}} G^{\mathrm{T}}$. In essence, [7] made the same observation, but we provide a simple

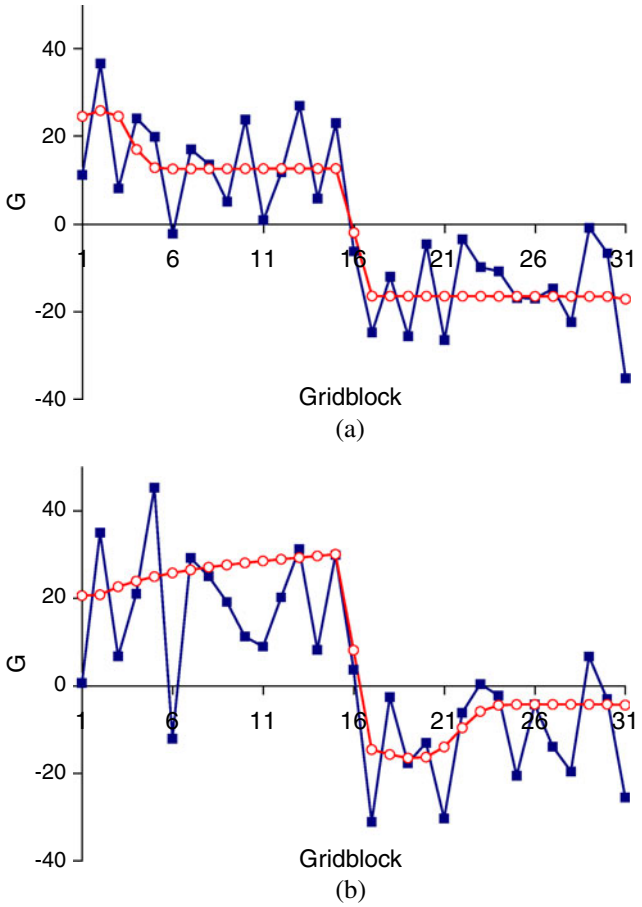

Fig. 27 Sensitivity obtained from EnRML (in *dark blue*) and the adjoint method (in *red*). **a** 30 days. **b** 360 days

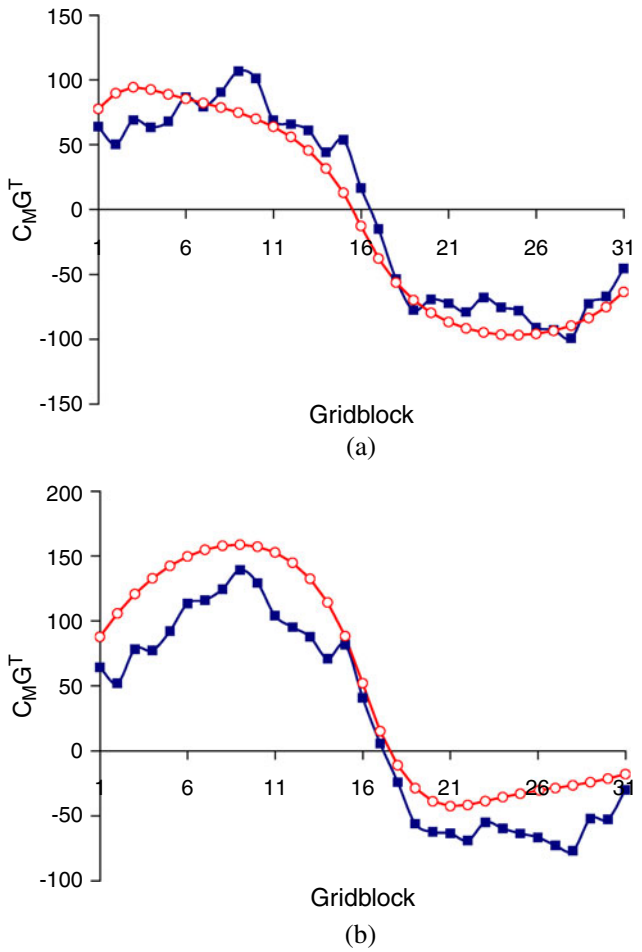

Fig. 28 Product of the prior covariance and transpose of sensitivity matrix obtained from EnRML (in *dark blue*) and the adjoint method (in *red*). **a** 30 days. **b** 360 days

theoretical explanation of why this occurs. In estimating $\widetilde{C}_{\mathrm{M}}^{\mathrm{f}}\widetilde{G}^{\mathrm{T}}$, we use

$$\widetilde{C}_{\mathrm{M}}^{\mathrm{f}} = \frac{1}{N_{\mathrm{e}}-1}\sum_{j=1}^{N_{\mathrm{e}}}\left(m_j^{\mathrm{f}}-\overline{m}^{\mathrm{f}}\right)\left(m_j^{\mathrm{f}}-\overline{m}^{\mathrm{f}}\right)^{\mathrm{T}} = \frac{1}{N_{\mathrm{e}}-1}\Delta M^{\mathrm{f}}\left(\Delta M^{\mathrm{f}}\right)^{\mathrm{T}}, \tag{30}$$

and from Eq. 29, we have

$$\left(\Delta D^{\ell}\right)^{\mathrm{T}} = \left(\Delta M^{\ell}\right)^{\mathrm{T}}\widetilde{G}_{\ell}^{\mathrm{T}}. \tag{31}$$

For the first iteration of EnRML, we have $\Delta M^{\ell} = \Delta M^{\mathrm{f}}$ and $\Delta D^{\ell} = \Delta D^{\mathrm{f}}$. Thus, multiplying $\widetilde{C}_{\mathrm{M}}^{\mathrm{f}}$ by $\widetilde{G}_{\ell}^{\mathrm{T}}$, we obtain

$$\begin{aligned}\widetilde{C}_{\mathrm{M}}^{\mathrm{f}}\widetilde{G}_{\ell}^{\mathrm{T}} &= \frac{1}{N_{\mathrm{e}}-1}\Delta M^{\mathrm{f}}\left(\Delta M^{\mathrm{f}}\right)^{\mathrm{T}}\widetilde{G}_{\ell}^{\mathrm{T}}\\ &= \frac{1}{N_{\mathrm{e}}-1}\Delta M^{\mathrm{f}}\left(\Delta D^{\mathrm{f}}\right)^{\mathrm{T}}\\ &= \widetilde{C}_{\mathrm{MD}}^{\mathrm{f}}.\end{aligned} \tag{32}$$

Therefore, the $\widetilde{C}_{\mathrm{M}}^{\mathrm{f}}\widetilde{G}_{\ell}^{\mathrm{T}}$ used in the first EnRML iteration is equal to $\widetilde{C}_{\mathrm{MD}}^{\mathrm{f}}$ used in EnKF and ES. Because Reynolds et al. [42] showed that $\widetilde{C}_{\mathrm{MD}}^{\mathrm{f}}$ can be approximated by $C_{\mathrm{M}}^{\mathrm{f}}\overline{G}_{\ell}^{\mathrm{T}}$, where $\overline{G}_{\ell}$ is the sensitivity matrix evaluated at $\overline{m}^{\mathrm{f}}$, it follows that $\widetilde{C}_{\mathrm{M}}^{\mathrm{f}}\widetilde{G}_{\ell}^{\mathrm{T}} \approx C_{\mathrm{M}}^{\mathrm{f}}\overline{G}_{\ell}^{\mathrm{T}}$ so that the approximation $\widetilde{C}_{\mathrm{M}}^{\mathrm{f}}\widetilde{G}_{\ell}^{\mathrm{T}}$ used in Eq. 28 should be reasonably accurate. Thus, the most unreliable approximation in Eq. 28 is the product $\widetilde{G}_{\ell}(m_j^{\ell}-m_j^{\mathrm{f}})$. However, the inaccuracy in $\widetilde{G}_{\ell}$ (Fig. 27) apparently is not bad enough to destroy the utility of the method.

In EnRML, all ensemble members are updated using the same average sensitivity matrix and step size. Unfortunately, there is no guarantee that the resulting search direction is downhill or the same step size is appropriate for all ensemble members. Figure 29 illustrates this fact for EnRML-S. In Fig. 29, we present the values of the normalized data mismatch objective function ($O_{\mathrm{N},d}$) for the first iteration considering different step sizes. Figure 29 shows that a step size $\beta_0 = 1$ cor-

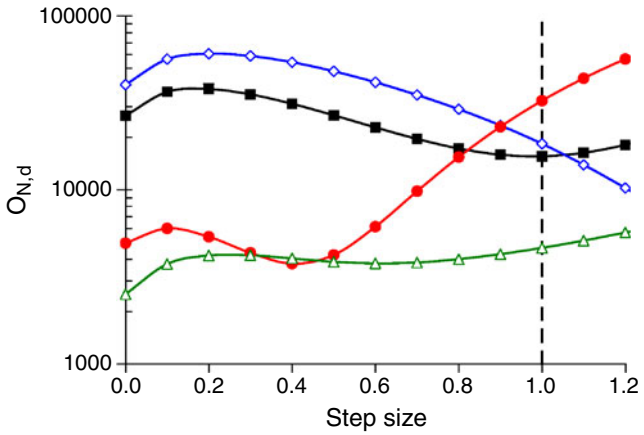

Fig. 29 Normalized data mismatch objective function versus step size for the first iteration of EnRML-S. This figure presents the values of $O_{N,d}$ for the mean (in *black*), first (in *blue*), third (in *red*), and 13th (in *green*) ensemble members. The *vertical dashed line* indicates the full step

responds to a decrease in the average $O_{N,d}$. Therefore, this step is accepted and used to update all ensemble members. However, Fig. 29 indicates that a step size of unity does not always yield a decrease in $O_{N,d}$ for all models. For example, $O_{N,d}$ increases for the third and 13th ensemble members. In fact, the search direction is not even downhill for the 13th ensemble member. A possible way to ameliorate this problem is to perform a different line search for each ensemble member as suggested by Wang et al. [56]. However, here, we tested only the original EnRML procedure proposed by Gu and Oliver [18].

We first considered the sequential formulation of EnRML (EnRML-F). However, we could not obtain reasonable data matches or estimates of the permeability field with this method. In our tests, EnRML-F failed to update model parameters for some consecutive data assimilation time steps because five cuts in the step size failed to give a decrease in $\overline{O}_d^{\ell+1}$. In other data assimilation time steps, EnRML-F resulted in apparent overcorrections of the permeability field. In most cases, these overcorrections occur after the eighth data assimilation time step, which corresponds to the water breakthrough in the monitor well. We tried different combinations of step sizes and termination criteria. We even tried to use a Levenberg–Marquardt update equation, instead of Gauss–Newton, to control the overcorrection issue. Despite these efforts, we could not match data with EnRML-F. Figure 30 shows the final permeability field obtained for the first ensemble with EnRML-F. This figure illustrates the overcorrections obtained in the permeability field close to the monitor well location.

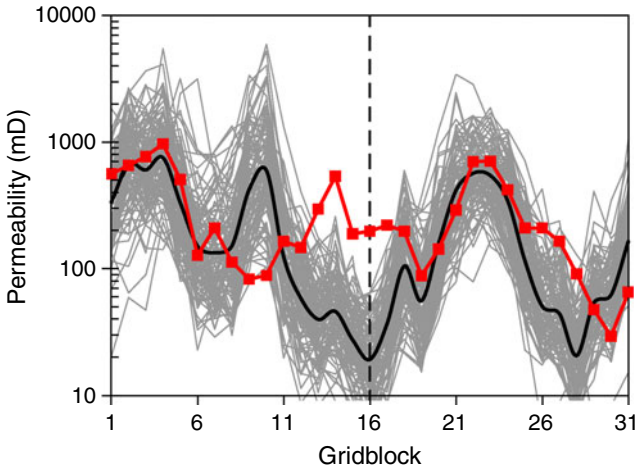

Fig. 30 Permeability fields after EnRML-F for the first ensemble

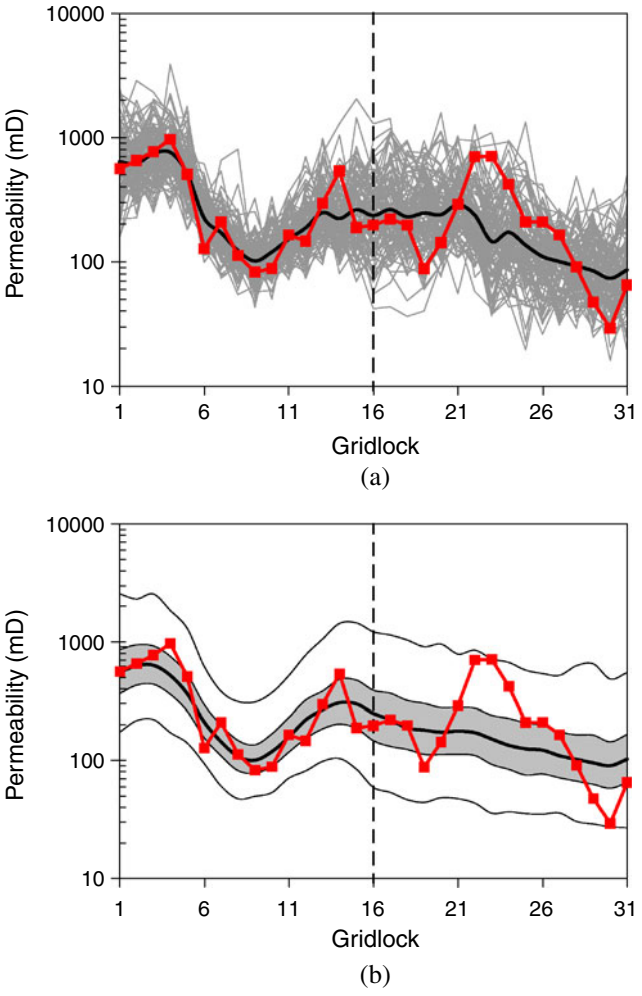

Fig. 31 Permeability fields after EnRML-S. **a** First ensemble. **b** All ensembles. The curves in this figure have the same meaning as in Fig. 5

For EnRML-S, on the other hand, we obtained more reasonable estimates of the permeability field. No overcorrection was observed in this case. Figure 31a presents the resulting permeability fields obtained by the first ensemble with EnRML-S while Fig. 31b presents the distribution of permeabilities obtained by combining the ten ensembles. Compared to MCMC, EnRML-S resulted in an acceptable permeability distribution although some overestimation in the spread is observed. In terms of predicted water production (Fig. 32), EnRML-S resulted in significant overestimation of uncertainty. Similar to the other ensemble-based methods, EnRML-S also obtained inconsistent distributions of W_p when repeating the data assimilation with ten different initial ensembles. Among the ten EnRML-S runs, eight stopped because of the maximum number of iterations, i.e., after ten iterations. This indicates that perhaps some improvements in the results of EnRML-S can be achieved if we allow more iterations. However, we limited the number of iterations to make the methods comparable in terms of computational cost. We also tried EnRML-S with an initial step size $\beta_0 = 0.5$, but we did not obtain significantly different results from the ones presented here, which use $\beta_0 = 1$.

15 Overall comparison

Figure 33 presents the values of the variance of log-permeability, var[ln(k)], after data assimilation for all methods considered in this paper. In order to make the results clear, we divided the results from the methods into two plots. We assume that MCMC results are correct, so we present the MCMC results in both plots of Fig. 33. According to the results in Fig. 33a, EnKF, DEnKF, HI-EnKF, LN-IEnKF, KHV-IEnKF, and ES gave unreasonably high values of var[ln(k)]. There are almost no differences between var[ln(k)] obtained with EnKF, HI-EnKF, and LN-IEnKF so that the corresponding curves overlap in Fig. 33a. Among all methods, KHV-IEnKF resulted in the largest overestimation of var[ln(k)]. According to the results in Fig. 33a, KHV-IEnKF obtained var[ln(k)] values larger than one for most of the reservoir gridblocks, i.e.,

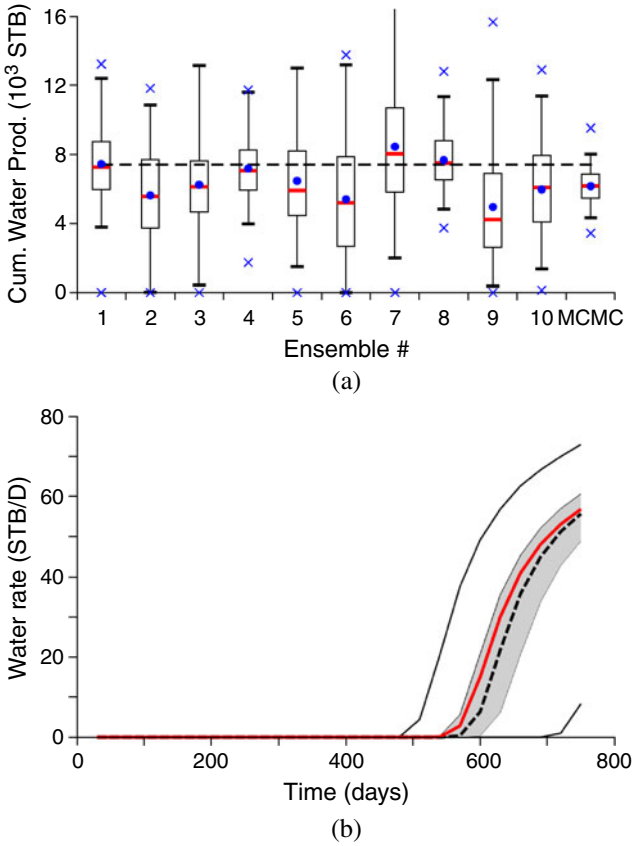

Fig. 32 Water production after EnRML-S. **a** Cumulative water production, W_p. **b** Water production rate, q_w. The colors in this figure have the same meaning as in Fig. 6

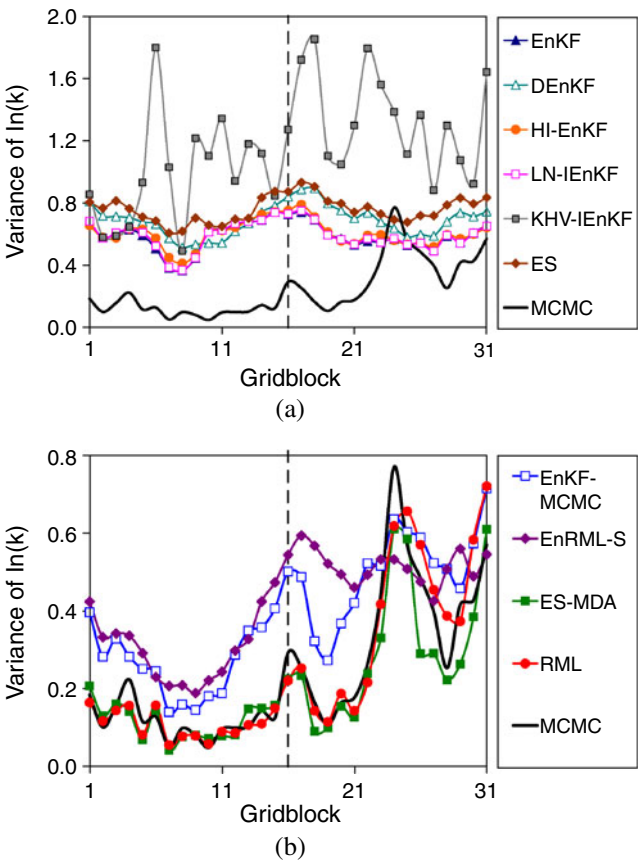

Fig. 33 Variance of log-permeability. Note that the vertical scale is different in each plot

variances higher than the prior variance. Figure 33b shows that, compared to each other, EnKF-MCMC and EnRML-S provided nearly identical values of var[ln(k)] for the gridblocks to the left of the monitor well and fairly similar variance values for the gridblocks to the right of the monitor well. However, EnKF-MCMC and EnRML-S overestimated the presumably correct variances obtained from MCMC although to a much lesser extent than the methods presented in Fig. 33a. The best results were obtained by ES-MDA and RML (Fig. 33b). These two methods resulted in values of var[ln(k)] very close to the ones obtained from MCMC for all gridblocks.

Figure 34 presents the values of the variance of the oil production rate, var[q_o], after data assimilation for all methods considered in this paper. We divided the results into three plots in order to make the figure clear and included the results from MCMC in all plots for comparison. EnKF, DEnKF, HI-EnKF, LN-IEnKF, KHV-IEnKF, and ES resulted in unreasonably high values of var[q_o] (Fig. 34a). EnKF-MCMC and EnRML-S overestimated the var[q_o] obtained from MCMC (Fig. 34b). However, after resampling, EnKF-MCMC resulted in var[q_o] fairly close to the variance obtained from MCMC although some overestimation is still observed for the forecast period. ES-MDA and RML resulted in values of var[q_o] in very good agreement with the results obtained from MCMC (Fig. 34c).

Figure 35 presents the box plots of O_N for all methods sorted in a decreasing order of O_N. In this test problem, we have 12 measurements and according to the criterion of Eq. 3, the values of O_N should be less than 3.06. However, only the RML and MCMC results satisfy this criterion. All other ensemble-based methods result in significantly higher values of the objective function. High values of the objective function are associated with poor data matches. More importantly, a model which results in high value of the objective function gives a small value of the posterior PDF, which suggests that this model is a sample from a low-probability region. Among the ensemble-based methods, ES-MDA obtains the lowest values of O_N. ES-MDA is also the ensemble-based method which gives the best quantification of uncertainty. In fact, there is a correlation between the reliability of the uncertainty quantification and the final values of O_N obtained by the ensemble-based methods. Note that EnKF, DEnKF, HI-EnKF, LN-IEnKF, KHV-InEnKF, and ES obtained very high values of O_N and resulted in unreasonably large overestimations of uncertainty. EnKF-MCMC, EnRML-S, ES-MDA, and RML give better data matches and a more reliable uncertainty quantification.

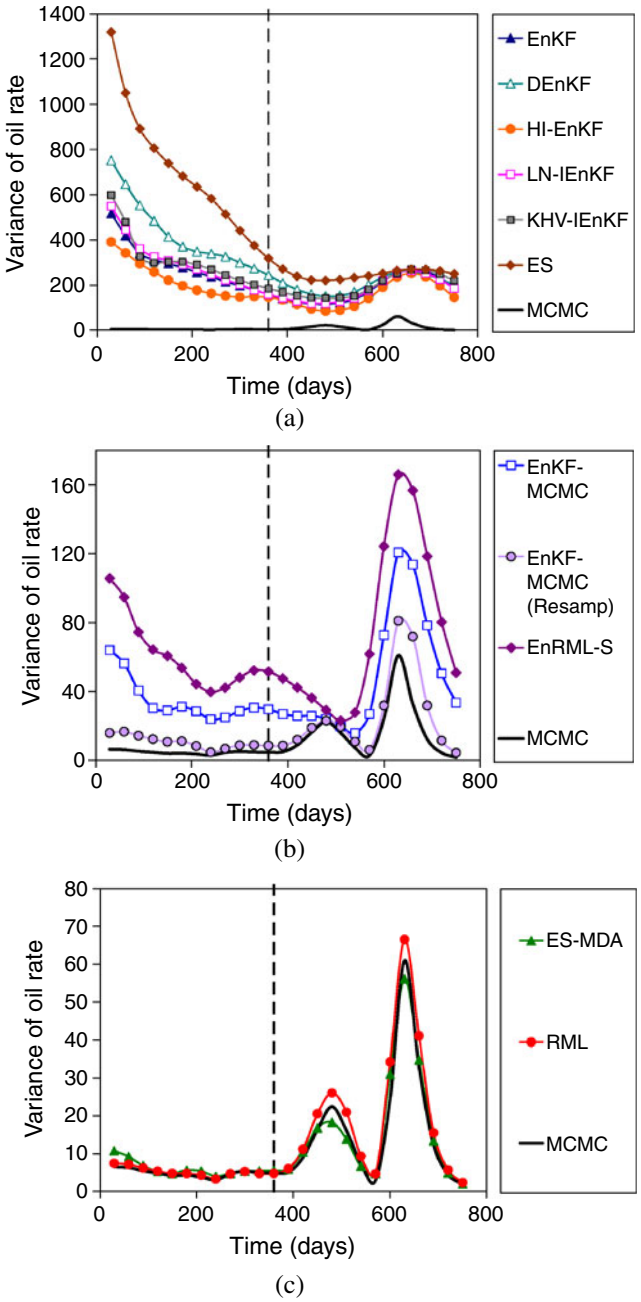

Fig. 34 Variance of oil production rate in stb^2/day^2. The *vertical dashed line* indicates the end of the period with observed data. Note that the vertical scale is different in each plot

Table 1 presents the estimated computational cost to generate an ensemble of 100 realizations with each method. However, because we have a very small simulation model, which requires about 0.2 s to run, the relative cost of writing/reading simulation files and matrix operations during the data assimilations becomes relatively important. Note that this is not the typical situation in reservoir history-matching problems where the CPU time required by the reservoir simulation

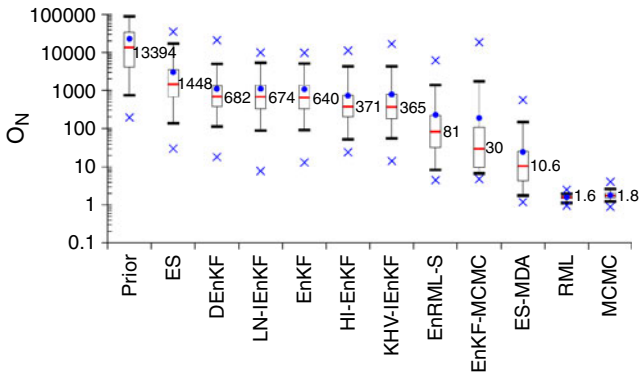

Fig. 35 Box plots of the normalized objective function. The *numbers* next to the boxes correspond to the median of O_N

largely dominates the total time of the data assimilation. For this reason, in Table 1, we present the computational time in terms of the total number of reservoir simulation runs and in terms of the actual measured CPU time divided by the measured CPU time of the ES method, which is the fastest method. Note that in the results of Table 1, one equivalent simulation run refers to the simulation of the total historical period; hence, we count 100 simulation runs for EnKF, even though these simulations require several restarts. According to the results in Table 1, ES is the fastest method in terms of both the number of reservoir simulation runs and the measured CPU time. Although EnKF also requires only 100 reservoir simulations, the total CPU time is 7.5 larger than ES mainly because of the simulation restarts. The same is true for the DEnKF. HI-EnKF requires running each reservoir simulation from time zero after each data assimilation, which makes the equivalent number of reservoir simulations 6.5 times higher than the number required by EnKF. For LN-IEnKF, the iterative process does not require additional reservoir simulations, but the total CPU time is longer than for EnKF because of the additional matrix operations required during the iterations. The computational cost of KHV-IEnKF corresponds to ten data assimilations with EnKF and ten reruns of the ensemble. For EnKF-MCMC, the total CPU time includes the time required for one data assimilation with EnKF, ten reruns of the ensemble, and the time required to generate the Markov chains. This makes the computational cost of EnKF-MCMC approximately 42 times the cost of data assimilation with ES. ES-MDA with ten data assimilations requires ten times the computational cost of ES. For EnRML-S, the iterative process often requires cutting the step size and rerunning the ensemble, which results in an average of 2,100 reservoir simulations per data assimilation and a total CPU time 37.8 times greater than that used with ES. For RML, each sample of the posterior PDF requires solving one minimization problem. In our implementation, each minimization requires, on average, 245 reservoir simulations. With RML, after each simulation, we also solve an adjoint problem to compute gradients [28]. Here, each adjoint solution requires on the order of 50 % of the time required for a simulation run. Therefore, the final CPU time for RML is 350 times the CPU time of ES. The computational cost for RML is very high for this test problem; however, the final objective function values obtained with RML are around 700 times lower than those from ES (the fastest method) or four times lower than those from ES-MDA (the ensemble-based method with the best performance). Moreover, RML is the only method which gives consistent sampling results between the ensembles, i.e., with RML, it would be sufficient to generate a single ensemble of 100 realizations instead of ten ensembles. For MCMC, we ran a very long chain with 20 million proposals. We did not measure the actual CPU time; however, it is clear that the direct application of MCMC for any reasonably sized reservoir model is not computationally feasible.

Table 1 Estimated computational cost to generate an ensemble of 100 realizations

Method	Equivalent number of simulation runs	Normalized CPU time
EnKF	100	7.5
DEnKF	100	7.0
HI-EnKF	650	12.9
LN-IEnKF	100	9.9
KHV-IEnKF	2,000	84.9
ES	100	1.0
ES-MDA	1,000	10.0
EnKF-MCMC	1,100	41.9
EnRML-S	2,100	37.8
RML	24,500	350.1
MCMC	2×10^6	–

Because the focus of these work was on sampling the posterior PDF and the size of the test problem was very small, we did not include any discussion on the computer storage requirements of the methods. However, RAM memory can be a relevant aspect especially for the application of the smoothers in problems with large amount of data, e.g., history matching of multiple seismic surveys. As the ensemble smoother with or without MDA requires assimilation of all data simultaneously and thus requires the inversion of a matrix (Eq. 3) of greater dimension than the matrix problem that must be solved with EnKF, i.e., the memory requirement is an even greater issue for the smoother than it is for EnKF. One way to reduce the memory requirements

when the matrix inverse in Eq. 3 is large is to apply a subspace inversion scheme [11, 13, 49].

16 Discussion and conclusions

In this paper, we compared one adjoint-based and nine ensemble-based methods in terms of the data matches, quantification of uncertainty, and computational cost for a small, but highly nonlinear, reservoir history-matching problem. The test problem was designed to be challenging for data assimilation such that the use of iterative schemes was necessary to achieve acceptable data matches. Among the ensemble-based methods considered, three (EnKF, DEnKF, and ES) are not iterative. Although we believe that conclusions 1–4, 6, and 9 are general, there is no assurance that any of the conclusions, enumerated below, especially those related to sampling accuracy, will generalize to larger more realistic reservoir problems. Nevertheless, based on the test problem, the following conclusions are warranted:

1. For strongly nonlinear problems, the noniterative methods (EnKF, ES, and DEnKF) do not result in acceptable history matches.
2. For strongly nonlinear problems, the noniterative methods (EnKF, ES, and DEnKF) do not provide acceptable approximations of the posterior PDF of model parameters and the posterior PDF of future performance predictions.
3. Because EnKF, ES, or DEnKF results in poor history matches, i.e., the ensemble spread in the matches obtained for each method is far too large, the uncertainty in future predicted performance is significantly overestimated.
4. Although HI-EnKF removes the parameter-state inconsistency during the data assimilation process, this desirable attribute is not always sufficient to significantly improve the history match or uncertainty estimates obtained with EnKF.
5. Although LN-IEnKF is an efficient iterative filter, for the example problem, it did not yield history matches and uncertainty estimates significantly different from those obtained with EnKF, and overall the performance of LN-IEnKF was slightly worse than the performance of HI-EnKF.
6. The KHV-IEnKF is based on a formulation which does not preserve statistical consistency of the Kalman filter for the linear-Gaussian case.
7. The KHV-IEnKF results in an incorrect posterior distribution of permeability.
8. Compared to the MCMC results, the history match and uncertainty quantification obtained with EnKF-MCMC and EnRML-S are acceptable, but for the test problem, the results were distinctly inferior to those obtained with ES-MDA. ES-MDA provided a quantification of uncertainty comparable to the adjoint-based RML if we combine the results of the ten data assimilations with different initial ensembles.
9. RML is the only method in the set considered that gives as good a data match as the one generated from MCMC.

Conclusion 3 is noteworthy because it is well known that EnKF can lead to underestimation of uncertainty in the model parameters and future predictions when the ensemble size is much smaller than the number of parameters that are estimated [1].

The data set used in this paper, including the reservoir simulator, the true permeability field, the ten initial ensembles, and the results from the long Markov chain are available for download at http://www.tuprep.utulsa.edu/comparative_study.html. The objective of this data set is to allow other research groups to reproduce the results in this paper, test their own implementations, and extend the comparative study to other methods not included in this paper. Note that one somewhat glaring omission of this paper is the two previous iteration methods that were codeveloped by the second author [27, 42]. These methods were not considered largely because they use an adjoint gradient and thus could do no better than RML in terms of estimating the posterior distributions. We also did not consider the parameter-state estimation scheme of [35] which has some remote similarities to HI-EnKF, the confirming step of [57], and the second iterative scheme of [27]. Also, as noted, we considered only one deterministic scheme, DEnKF. As ensemble-based methods are an active area of research, we also expect that more iterative methods will be developed in the near future. In such an event, we hope that other research groups will expand the comparison presented in this paper.

Acknowledgements The support of the member companies of TUPREP is gratefully acknowledged. The first author acknowledges the financial support from Petrobras.

References

1. Aanonsen, S.I., Nævdal, G., Oliver, D.S., Reynolds, A.C., Vallés, B.: Review of ensemble Kalman filter in petroleum engineering. Soc. Pet. Eng. J. **14**(3), 393–412 (2009)
2. Anderson, J.L., Anderson, S.L.: A Monte Carlo implementation of the nonlinear filtering problem to produce

ensemble assimilations and forecasts. Mon. Weather Rev. **127**(12), 2741–2758 (1999)
3. Bonet-Cunha, L., Oliver, D.S., Rednar, R.A., Reynolds, A.C.: A hybrid Markov chain Monte Carlo method for generating permeability fields conditioned to multiwell pressure data and prior information. Soc. Pet. Eng. J. **11**(3), 261–271 (1998)
4. Burgers, G., van Leeuwen, P., Evensen, G.: Analysis scheme in the ensemble Kalman filter. Mon. Weather Rev. **126**(6), 1719–1724 (1998)
5. Chavent, G.M., Dupuy, M., Lemonnier, P.: History matching by use of optimal control theory. Soc. Pet. Eng. J. **15**(1), 74–86 (1975)
6. Chen, W.H., Gavalas, G.R., Seinfeld, J.H., Wasserman, M.L.: A new algorithm for automatic history matching. Soc. Pet. Eng. J. **14**(6), 593–608 (1974)
7. Chen, Y., Oliver, D.: Ensemble randomized maximum likelihood method as an iterative ensemble smoother. Math. Geosci. **44**(1), 1–26 (2011)
8. de Marsily, G., Lavedan, G., Boucher, M., Fasanino, G.: Interpretation of interference tests in a well field using geostatistical techniques to fit the permeability distribution in a reservoir model. In: Verly, G., David, M., Journel, A.G., and Marechal, A. (eds.) Geostatistics for Natural Resources Characterization, Part 2, pp. 831–849. D. Reidell, Dordrecht (1984)
9. Emerick, A.A., Reynolds, A.C.: Combining the ensemble Kalman filter with Markov chain Monte Carlo for improved history matching and uncertainty characterization. Soc. Pet. Eng. J. **17**(2), 418–440 (2012a)
10. Emerick, A.A., Reynolds, A.C.: Ensemble smoother with multiple data assimilation. Computers & Geosciences (2012b). doi:10.1016/j.cageo.2012.03.011
11. Emerick, A.A., Reynolds, A.C.: History matching time-lapse seismic data using the ensemble Kalman filter with multiple data assimilations. Comput. Geosci **16**(3), 639–659 (2012c)
12. Evensen, G.: Sequential data assimilation with a nonlinear quasi-geostrophic model using Monte Carlo methods to forecast error statistics. J. Geophys. Res. **99**(C5), 10,143–10,162 (1994)
13. Evensen, G.: Sampling strategies and square root analysis schemes for the EnKF. Ocean Dyn. **54**(6), 539–560 (2004)
14. Evensen, G.: The ensemble Kalman filter for combined state and parameter estimation. In: IEEE Control Systems Magazine, pp. 83–104 (2009)
15. Gao, G., Reynolds, A.C.: An improved implementation of the LBFGS algorithm for automatic history matching. Soc. Pet. Eng. J. **11**(1), 5–17 (2006)
16. Gao, G., Zafari, M., Reynolds, A.C.: Quantifying uncertainty for the PUNQ-S3 problem in a Bayesian setting with RML and EnKF. Soc. Pet. Eng. J. **11**(4), 506–515 (2006)
17. Gelman, A., Roberts, G.O., Gilks, W.R.: Efficient Metropolis jumping rules. Bayesian Stat. Oxford University Press **5**(5), 599–607 (1996)
18. Gu, Y., Oliver, D.S.: An iterative ensemble Kalman filter for multiphase fluid flow data assimilation. Soc. Pet. Eng. J. **12**(4), 438–446 (2007)
19. Hastings, W.K.: Monte Carlo sampling methods using Markov chains and their applications. Biometrika **57**(1), 97–109 (1970)
20. Houtekamer, P.L., Mitchell, H.L.: Data assimilation using an ensemble Kalman filter technique. Mon. Weather Rev. **126**(3), 796–811 (1998)
21. Houtekamer, P.L., Mitchell, H.L.: A sequential ensemble Kalman filter for atmospheric data assimilation. Mon. Weather Rev. **129**(1), 123–137 (2001)
22. Hu, L.Y.: Gradual deformation and iterative calibration of Gaussian-related stochastic models. Math. Geol. **32**(1), 87–108 (2000)
23. Kitanidis, P.K.: Quasi-linear geostatistical theory for inversing. Water Resour. Res. **31**(10), 2411–2419 (1995)
24. Krymskaya, M.V., Hanea, R.G., Verlaan, M.: An iterative ensemble Kalman filter for reservoir engineering applications. Comput. Geosci **13**(2), 235–244 (2009)
25. LaVenue, A.M., Pickens, J.F.: Application of a coupled adjoint sensitivity and kriging approach to calibrate a groundwater flow model. Water Resour. Res. **28**(6), 1543–1569 (1992)
26. LaVenue, A.M., RamaRao, B.S., de Marsily, G., Marietta, M.G.: Pilot point methodology for automated calibration of an ensemble of conditionally simulated transmissivity fields, 2. Application, Water Resour. Res. **31**(3), 495–516 (1995)
27. Li, G., Reynolds, A.C.: Iterative ensemble Kalman filters for data assimilation. Soc. Pet. Eng. J. **14**(3), 496–505 (2009)
28. Li, R., Reynolds, A.C., Oliver, D.S.: History matching of three-phase flow production data. Soc. Pet. Eng. J. **8**(4), 328–340 (2003)
29. Liu, D., Nocedal, J.: On the limited memory BFGS method for large scale optimization. Math. Program. **45**, 503–528 (1989)
30. Liu, N.: Assessment of Uncertainty Assessment Methods. Master's thesis, The University of Tulsa, Tulsa, Oklahoma (2002)
31. Liu, N., Oliver, D.S.: Evaluation of Monte Carlo methods for assessing uncertainty. Soc. Pet. Eng. J. **8**(2), 188–195 (2003)
32. Lorentzen, R.J., Nævdal, G.: An iterative ensemble Kalman filter. IEEE Trans. Automat. Contr. **56**(8), 1990–1995 (2011)
33. Lorentzen, R.J., Nævdal, G., Vallès, B., Berg, A.M., Grimstad, A.-A.: Analysis of the ensemble Kalman filter for estimation of permeability and porosity in reservoir models. In: Proceedings of the SPE Annual Technical Conference and Exhibition, Dallas, TX, SPE 96375, 9–12 October 2005
34. Metropolis, N., Rosenbluth, A.W., Rosenbluth, M.N., Teller, A.H., Teller, E.: Equations of state calculations by fast computing machines. J. Chem. Phys. **21**, 1087–1092 (1953)
35. Moradkhani, H., Sorooshian, S., Gupta, H.V., Mouser, P.R.: Dual state-parameter estimation of hydrological models using ensemble Kalman filter. Adv. Water Resour. **28**(2), 301–305 (2005)
36. Nocedal, J.: Updating quasi-Newton matrices with limited storage. Math. Comput. **35**(151), 773–782 (1980)
37. Oliver, D.S., Cunha, L.B., Reynolds, A.C.: Markov chain Monte Carlo methods for conditioning a permeability field to pressure data. Math. Geol. **29**(1), 61–91 (1997)
38. Oliver, D.S., He, N., Reynolds, A.C.: Conditioning permeability fields to pressure data. In: Proceedings of the European Conference for the Mathematics of Oil Recovery (1996)
39. Oliver, D.S., Reynolds, A.C., Liu, N.: Inverse Theory for Petroleum Reservoir Characterization and History Matching. Cambridge University Press, Cambridge (2008)
40. Peaceman, D.W.: Interpretation of well-block pressures in numerical reservoir simulation with non-square grid blocks and anisotropic permeability. Soc. Pet. Eng. J. **23**(6), 531–543 (1983)
41. Reynolds, A.C., He, N., Oliver, D.S.: Reducing uncertainty in geostatistical description with well testing pressure data. In: Schatzinger, R.A., Jordan, J.F. (eds.) Reservoir Characterization—Recent Advances, pp. 149–162. AAPG Memoir 71, Tulsa (1999)

42. Reynolds, A.C., Zafari, M., Li, G.: Iterative forms of the ensemble Kalman filter. In: Proceedings of 10th European Conference on the Mathematics of Oil Recovery, Amsterdam, 4–7 September 2006
43. Roberts, G.O., Gelman, A., Gilks, W.R.: Weak convergence and optimal scaling of random walk Metropolis algorithm. Ann. Appl. Probab. **7**(1), 110–120 (1997)
44. Roberts, G.O., Rosenthal, J.S.: Optimal scaling of various Metropolis-Hastings algorithms. Stat. Sci. **16**(4), 351–367 (2001)
45. Roggero, F., Hu, L.Y.: Gradual deformation of continuous geostatistical models for history matching. In: Proceedings of the SPE Annual Technical Conference and Exhibition, New Orleans, LA, SPE 49004, 27–30 September 1998
46. Sakov, P., Bertino, L.: Relation between two common localisation methods for the EnKF. Comput. Geosci **15**(2), 225–237(2011)
47. Sakov, P., Oke, P.R.: A deterministic formulation of the ensemble Kalman filter: an alternative to ensemble square root filters. Tellus, Ser. A Dyn. Meteorol. Oceanogr. **60**(2), 361–371 (2008a)
48. Sakov, P., Oke, P.R.: Implications of the form of the ensemble transformation in the ensemble square root filters. Mon. Weather Rev. **136**, 1042–1053 (2008b)
49. Skjervheim, J.-A., Evensen, G., Aanonsen, S.I., Ruud, B.O., Johansen, T.A.: Incorporating 4D seismic data in reservoir simulation models using ensemble Kalman filter. Soc. Pet. Eng. J. **12**(3), 282–292 (2007)
50. Sun, A.Y., Morris, A., Mohanty, S.: Comparison of deterministic ensemble Kalman filters for assimilating hydrogeological data. Adv. Water Resour. **32**, 280–292 (2009)
51. Tavakoli, R., Reynolds, A.A.: Monte Carlo simulation of permeability fields and reservoir performance predictions with SVD parameterization in RML compared with EnKF. Comput. Geosci. **15**(1), 99–116 (2011)
52. Thulin, K., Li, G., Aanonsen, S.I., Reynolds, A.C.: Estimation of initial fluid contacts by assimilation of production data with EnKF. In: Proceedings of the SPE Annual Technical Conference and Exhibition, Anaheim, CA, SPE 109975, 11–14 November 2007
53. Thulin, K., Nævdal, G., Skaug, H.J., Aanonsen, S.I.: Quantifying Monte Carlo uncertainty in the ensemble Kalman field. Soc. Pet. Eng. J. **16**(1), 172–182 (2011)
54. Tippett, M.K., Anderson, J.L., Bishop, C.H., Hamill, T.M., Whitaker, J.S.: Ensemble square-root filters. Mon. Weather Rev. **131**, 1485–1490 (2003)
55. van Leeuwen, P.J., Evensen, G.: Data assimilation and inverse methods in terms of a probabilistic formulation. Mon. Weather Rev. **124**, 2898–2913 (1996)
56. Wang, Y., Li, G., Reynolds, A.C.: Estimation of depths of fluid contacts by history matching using iterative ensemble-Kalman smoothers. Soc. Pet. Eng. J. **15**(2) (2010)
57. Wen, X.-H., Chen, W.H.: Real-time reservoir model updating using ensemble Kalman filter with confirming option. Soc. Pet. Eng. J. **11**(4), 431–442 (2006)
58. Wu, Z., Reynolds, A.C., Oliver, D.S.: Conditioning geostatistical models to two-phase production data. Soc. Pet. Eng. J. **3**(2), 142–155 (1999)
59. Zafari, M., Reynolds, A.C.: Assessing the uncertainty in reservoir description and performance predictions with the ensemble Kalman filter. Soc. Pet. Eng. J. **12**(3), 382–391 (2007)
60. Zhang, F., Reynolds, A.C.: Optimization algorithms for automatic history matching of production data. In: Proceedings of 8th European Conference on the Mathematics of Oil Recovery, Freiberg, Germany, 3–6 September 2002